Biochemical, structural, and functional studies reveal that MAB_4324c from Mycobacterium abscessus is an active tandem repeat N -acetyltransferase

Husam M.A.B. Alsarraf, Kien Lam Ung, Matt Johansen, Juliette Dimon, Vincent Olieric, Laurent Kremer, Mickaël Blaise

Biochemical, structural, and functional studies reveal that MAB_4324c from *Mycobacterium abscessus* is an active tandem repeat *N*-acetyltransferase

Running Title: MAB_4324c is an atypical *N*-acetyltransferase

Husam M.A.B. Alsarraf[1,2], Kien Lam Ung[1#], Matt D. Johansen[1$], Juliette Dimon[1], Vincent Olieric[3], Laurent Kremer[1,4] and Mickaël Blaise[1,*]

1 IRIM, Université de Montpellier, CNRS, Montpellier, France.
2 Department of Molecular Biology and Genetics, Aarhus University, Aarhus, Denmark
3 Swiss Light Source, Paul Scherrer Institute, CH-5232 Villigen-PSI, Switzerland.
4 INSERM, IRIM, Montpellier, France.
$ Present address: Centre for Inflammation, Centenary Institute and University of Technology Sydney, Faculty of Science, School of Life Sciences, Sydney, NSW, Australia.
# Present address: Department of molecular biology and Genetics, Aarhus University, Aarhus, Denmark
* Correspondence: mickael.blaise@irim.cnrs.fr

Abstract

Mycobacterium abscessus is a pathogenic non-tuberculous mycobacterium that possesses an intrinsic drug-resistance profile. Several *N*-acetyltransferases mediate drug resistance and/or participate in *M. abscessus* virulence. Mining the *M. abscessus* genome has revealed genes encoding additional *N*-acetyltransferases whose functions remain uncharacterized, of which MAB_4324c is among them. We showed that the MAB_4324c protein is an *N*-acetyltransferase able to acetylate polyamine substrates. The crystal structure of MAB_4324c was solved at high resolution in complex with its cofactor, revealing the presence of two GCN5-related *N*-acetyltransferase domains and a cryptic binding site for NADPH. Genetic studies demonstrate that *MAB_4324c* is not essential for *in vitro* growth of *M. abscessus*, however overexpression of the protein enhanced the uptake and survival of *M. abscessus* in THP-1 macrophages.

Keywords: *Mycobacterium abscessus*, *N*-acetyltransferase, GCN5, X-ray structure, macrophage, infection, intracellular survival.

Abbreviations

Mab, *Mycobacterium abscessus*; CF, Cystic Fibrosis; MmpS, Mycobacterial membrane protein small; MmpL, Mycobacterial membrane protein large; GNAT, GNC5-related *N*-acetyltransferase; Eis, Enhanced in intracellular survival; TEV, Tobacco Etch Virus; Isopropyl-*β*-D-thiogalactoside, IPTG; SEC, size-exclusion chromatography; Polyethylene glycol, PEG; *β*-mercaptoethanol, *β*-ME; DTNB, 5,5-dithio-bis-(nitrobenzoic acid; OADC, oleic acid-albumin-dextrose-catalase; KAN, kanamycin; AMK, amikacin; apramycin, APR; hygromycin B, HYG; tyramine, TYR; spermine, SPR; spermidine, SPDN; acetyl-CoA, ACO; coenzyme A, CoA; NADH, reduced nicotinamide adenine dinucleotide; NADPH, reduced nicotinamide adenine dinucleotide phosphate; ADP, adenosine diphosphate; colony-forming units, CFU; WT, wild-type;

Introduction

Mycobacterium abscessus (Mab) is an opportunistic non-tuberculous human pathogen [1]. The *Mycobacterium abscessus* complex encompasses three subspecies *M. abscessus sensu stricto*, *M. abscessus* subsp. *massiliense* and *M. abscessus* subsp. *bolletii*. Several epidemiological studies have emphasized a possible human-human transmission cycle of Mab [2,3], and demonstrated that only a few dominant clones are circulating [4], which is in favor of global transmission of Mab in humans. The prevalence of Mab pulmonary infection was estimated to be below 1 per 100000 inhabitants in the United States, however this number might be underestimated and Mab infections are expected to be on the rise [5]. Patients with underlying genetic and structural abnormalities, such as those with bronchiectasis or CF are particularly susceptible to Mab infection[1]. The prevalence of Mab infection among CF patients is estimated to range from 5 to 20% [6]. Treatments of Mab infections are particularly long and are often associated with therapeutic failures. The poor efficacy of drug treatments is correlated with the intrinsic resistance of Mab to most common antibiotics, including first-line anti-tubercular isoniazid and rifampicin [1,7]. In addition to the low permeability of the mycobacterial cell wall which limits the penetration of small molecules, Mab has developed multiple resistance mechanisms that include drug efflux activity mediated by MmpS/MmpL transporters [8,9], modifications or hydrolysis of the drug [7,10–15], and/or alteration of the drug target [16,17] ultimately incapacitating drug activity.

Mab is thought to be an environmental bacterium that colonizes different hosts and can persist within amoebae [18]. While Mab can replicate within amoeba, genomic analyses highlighted the accumulation of non-mycobacterial genes, which are thought to have been acquired to promote environmental persistence and nutrient acquisition. Furthermore, thorough transcriptomic analyses deciphered the differential gene expression pattern in correlation with the lifestyle of Mab, and

identified several genes which were shown to be up-regulated when Mab is inside amoebae or in murine macrophages, thus highlighting the occurrence of an adaptive transcriptional program in response to various stresses encountered within the cell [19]. To this end, the *MAB_4532c* gene, encoding the Eis2 protein, plays a critical role in the intramacrophage survival of Mab [19]. Eis proteins that belong to the GNAT family indeed play a key role in the intracellular survival of other pathogenic mycobacteria and notably *Mycobacterium tuberculosis* [20,21]. In addition, due to their *N*-acetyltransferase activity, Eis proteins can modify aminoglycoside antibiotics through acetylation, thereby impairing their binding to the ribosomes and leading to drug resistance [22,23]. Moreover, Eis2 confers high-level resistance to aminoglycosides in Mab [12–14]. A very close homologue of Eis2, named Eis1, is neither required for intracellular survival [19] nor aminoglycoside resistance, suggesting that it possesses another function that remains to be defined [12,14]. Together, these findings exemplify the need to experimentally address the substrate specificity and biological function of GNAT proteins despite their high homology levels with well-described homologues.

Transcriptomic approaches have been largely employed to identify key players of the drug resistance and/or virulence response in mycobacteria. As such, gene regulation studies have revealed that *MAB_4324c* is more highly expressed under intracellular growth conditions as compared to planktonic cultures [19]. In contrast, *MAB_4324c* expression is down-regulated in a Mab *whiB7* deletion mutant [15]. WhiB7 represents a master transcription regulator controlling gene expression involved in the stress response and confers resistance to several classes of antibiotics, opening up the possibility that *MAB_4324c* might participate in these processes. Furthermore, RNAseq analyses identified several genes including *MAB_4324c* that were up-regulated upon exposure of Mab to clinically-relevant antibiotics, such as amikacin, clarithromycin, and tigecycline [24].

Considering the importance of GNAT enzymes in mycobacterial drug-resistance mechanisms and virulence, and because MAB_4324c encodes a predicted GNAT, this study was undertaken to functionally characterize the role of MAB_4324c in Mab. Herein, a combination of biochemical and structural approaches was used to demonstrate that MAB_4324c is an active tandem repeat *N*-acetyltransferase. Genetic studies showed that while MAB_4324c is dispensable for planktonic growth, its overexpression confers an intracellular growth advantage to Mab in THP-1 macrophages.

Materials and Methods

MAB_4324c cloning into the expression plasmid

The *MAB_4324c* gene was synthesized by Genscript with codon-optimized for *Escherichia coli* expression and cloned into the expression vector pET-30a. The sequences encoding for the hexahistidine- and S-tags followed by the TEV protease site were included in the 5'-end of the gene.

MAB_4324c expression and purification

The pET30a::*MAB_4324c* construct was transformed into *E. coli* BL21 (DE3) resistant to Phage T1 (New England Biolabs) and then transformed with the pRARE2 plasmid encoding rare tRNAs. An overnight pre-culture was used to inoculate a 12L culture of Luria broth (LB) media supplemented with 50 µg.mL^{-1} and 30 µg.mL^{-1} of KAN and chloramphenicol. The culture was grown until the exponential growth phase was reached and subjected to cold shock in an ice bath before induction of the protein expression with 1mM of IPTG (Euromedex) overnight at 18ºC. The bacteria were homogenized in lysis buffer A (50 mM Tris-HCl pH 8, 0.4 M NaCl, 20 mM imidazole, 1 mM benzamidine and 5 mM β-ME). Bacteria were disrupted by sonication and centrifugated at 28000 *g*. The soluble fraction was loaded onto a Ni-NTA Sepharose resin (Cytiva) by gravity. The column was washed with buffer A and buffer B (50 mM Tris-HCl pH 8, 1M NaCl and 5 mM β-ME). Proteins were eluted with buffer C (50 mM Tris-HCl pH 8, 0.2 M NaCl, 5 mM β-ME and 400 mM imidazole). The eluate was dialyzed overnight at 4ºC in dialysis buffer D (50 mM Tris-HCl pH 8, 0.2 M NaCl and 5 mM β-ME) in the presence of His-tagged TEV protease in a 50:1 w/w ratio to remove the tags. The TEV protease and the uncleaved MAB_4324c were separated from the untagged proteins by the passage of the dialyzed eluate through a Ni-NTA sepharose column. MAB_4324c was collected in the flow-through and concentrated by ultra-filtration (centricon 10 kDa CW-Sartorius). Finally, MAB_4324c was concentrated to 5mg.mL^{-1} and loaded onto a size-exclusion chromatography (SEC) column (Superdex 200 Increase 10/300 column from GE Cytiva) and eluted with buffer E (20 mM Tris-HCl pH 7.4 and 0.2 M NaCl).

Determination of MAB_4324c oligomeric by size-exclusion chromatography

The Superdex 200 Increase 10/300 GL column (Cytiva) was calibrated with the Gel Filtration Markers Kit for protein molecular weight (MW) ranging from 12 400 to 200 000 Da (Sigma-Aldrich). The MW markers and MAB_4324c were eluted with buffer E as described above and at a flow rate of 0.4 mL.min^{-1} at 8ºC. The partition coefficient (K_{av}) of each protein was calculated with the following formula K_{av}=(Ve-V0/Vt-V0) where Ve is the volume of elution of the proteins, Vt the volume of the column (24 mL) and V0 the void volume corresponding to the

elution volume of dextran blue. The MW of MAB_4324c was extrapolated from the semi-logarithmic plot of the partition coefficients, K_{av}, of the standard proteins marker versus their respective molecular masses on a logarithmic scale.

Crystallization

MAB_4324c crystals were grown in sitting drops using the MR Crystallization Plates™ (Hampton Research) at 18ºC by mixing 1 µL of 12 mg.mL^{-1} protein supplemented with 2 mM acetyl-CoA (incubated for 1h on ice), with 1 µL of reservoir solution (2 M ammonium sulfate, 0.1 M HEPES pH 7.5 and 2% w/v PEG400). Cryoprotection was not employed before crystals were cryo-cooled in liquid nitrogen, as all cryoprotective conditions tested led to crystal damage. Consequently, ice rings were present on diffraction data but did not affect data processing or structure refinement.

Data collection, structure determination and, refinement

X-ray data collection was performed at the X06DA-PXIII beamline at the Swiss Light Source **(Table II)**. A 360° native data set was collected at a wavelength of 1-Å with an oscillation of 0.2° and an exposure time of 0.1 s on PILATUS 2M-F detector [25]. A single-wavelength anomalous diffraction experiment from intrinsic sulfur atoms (S-SAD) consisting of 12 × 360° ω scans at varying values of χ and φ of the PRIGo multi-axis goniometer [26], was collected on a single crystal at 100 K at 2.075-Å wavelength using 0.2° oscillation 0.1 s exposure as previously described [27]. Data processing, scaling and merging were performed using *XDS* and *XSCALE* [28]. The high-resolution data cutoff was based on the statistical indicators $CC_{1/2}$ [29]. Substructure determination and phasing were performed with *SHELX* [30,31] using the *CRANK2* program [32]. The automatically built model using *CRANK2* was rebuilt with *Coot* [33] and refined with *Phenix* [34] against the native data set **(Table II)**. The structure factors and atomic coordinates were deposited at the Protein Data Bank under the accession entry 7Q3A.

Kinetics assay

MAB_4324c was concentrated to 7.5 mg.mL^{-1} in buffer E supplemented with 50% glycerol for use in kinetic assays. The reaction was performed at 25ºC in a quartz cuvette and consisted of monitoring the production of 2-thio-5-nitrobenzoic acid (TNB; extinction coefficient of 14150 M^{-1} cm^{-1} at 412 nm) resulting in the reduction of DTNB by the free CoA. Data points were recorded with a time interval of 5 sec for 50 to 60 sec using a Nanodrop2000c spectrophotometer (ThermoFisher Scientific). All compounds and the enzyme were dissolved and diluted in buffer E. MAB_4324c (0.25 µM) was added to the reaction mixture consisting of DTNB (0.5 mM), ACO

(0.5 mM) as well as substrates when requested in a final volume of 100 µL. A reaction mixture lacking the substrate was used to determine the reaction background and to normalize the values. Standard errors were calculated from triplicates and a nonlinear least-squares regression algorithm was used to determine the Michaelis-Menten equation (GraphPad Prism software).

Generation of an unmarked *MAB_4324c* knockout mutant in *M. abscessus.*

The Δ*MAB_4324c M. abscessus* strain was generated by the unmarked deletion strategy involving two recombination steps as described previously [35]. The *MAB_4324c* (1059 bp) flanking regions (each around 1500 bp) were PCR-amplified using the Phusion polymerase (ThermoFisher Scientific) and the following primers (upstream region FW: 5'-CCGGCTAGCTTCGTCAACAAGAAACTCATCCGCACCCTGTGAGCCAG-3', upstream region RV: 5'-GTCGCAAATAGGGTTGAACCCATGACATCCCACACGCAATTGGTGAACCGTTCGATCAG CCTGATCAAACAGTTC-3', downstream region FW: 5'-GAACTGTTTGATCAGGCTGATCGAACGGTTCACCAATTGCGTGTGGGATGTCATGGGTT CAACCCTATTTGCGAC-3', downstream region RV: 5'-ACCGTTAACGCTGACGGGCGGGTTCAGAGTGAAGGT-3'). Amplicons were purified and treated with restriction enzymes (all from NewEngland Biolabs), ligated into pUX1-*katG*$_{Mtb,\ and}$ digested with NheI and HpaI restriction sites, where the flanking regions were ligated at the MfeI restriction site.

The resulting plasmid was transformed into electro-competent Mab CIP104536T, smooth variant [18]. Transformed bacteria were placed at 37ºC for 3 hrs under agitation before plating on Middlebrook 7H10 (BD Difco) supplemented with oleic acid-albumin-dextrose-catalase (OADC) enrichment (7H10^{OADC}) and 250 µg.mL^{-1} KAN. The selection of colonies was based on resistance to KAN and tdTomato expression (red fluorescent colonies) as an indicator for the first recombination event. Selected red colonies were grown after 4 days in Middlebrook 7H9 broth (BD Difco) supplemented with OADC, 0.025% tyloxapol and 250 µg.mL^{-1} KAN. Bacteria were pelleted, washed thrice and resuspended in an antibiotic-free medium. Cultures were then incubated overnight at 37ºC under agitation to allow for the second recombination event to occur. Bacteria were then plated on 7H10^{OADC} plates supplemented with 50 µg.mL^{-1} isoniazid (INH) and incubated at 37ºC for 4 days. INH-resistant and non-fluorescent colonies were genotyped by PCR to identify the mutants. Proper gene deletion was subsequently confirmed by PCR and sequencing.

Overexpression of *MAB_4324c* in *M. abscessus*.

MAB_4324c was amplified by PCR from genomic DNA using the following primers, Fw: 5'-AACGAATTCATGACATCCCACACGGTACCGACGGC-3', Rv:-5' CGCGTTAACTCACTTCTCGAACTGCGGGTGGCTCCAGAACTGTTTGATCAGGCTGATCG AACGGTT-3', (restriction sites are underlined) and cloned into the episomal pMV261 [36] and into integrative pMV306 both cut with EcoRI and HpaI. This cloning strategy allows gene expression under the control of the strong *hsp60* promoter. The cloning strategy enabled the addition of a strep tag at the C-terminus of MAB_4324c. The pMV261::*MAB_4324c* and pMV306::*MAB_4324c* construct were introduced into electro-competent Mab WT and Δ*MAB_4324c* strains. The transformed bacteria were plated on $7H10^{OADC}$ agar containing 250 µg.mL^{-1} KAN. Individual colonies were then grown in 10 mL of Middlebrook $7H9^{OADC}$supplemented with 0.025% tyloxapol and 250 µg.mL^{-1} KAN at 37ºC for 4 days, harvested and frozen at -80ºC.

Assessment of protein expression by Western blotting

Bacteria were disrupted by bead-beating, sonication and centrifuged at 20 000 *g*, at 4 ºC. The total proteins from the crude extract (about 100 µg) were separated by SDS-PAGE, and were then blotted onto a nitrocellulose membrane (Cytiva) in transfer buffer (20 mM Tris, 150 mM glycine and 10 to 20% (v/v) ethanol). The membrane was treated with blocking buffer: PBS 1X, 5% (w/v) skimmed milk and 0.2% (v/v) Tween 20. Membranes were first incubated either with a primary anti-Strep-tag monoclonal antibody (dilution 1/10000; Sigma-Aldrich) or with a rabbit anti-acetyl lysine primary antibody (dilution 1/500-1/1000; abcam21623) and subsequently incubated with a secondary anti-mouse monoclonal antibody or an anti-rabbit antibody conjugated to the horseradish peroxidase (dilution 1/2000-1/5000; Sigma-Aldrich). Immunoreactive bands were revealed using the luminol-based reaction (SuperSignalTM–Thermo Fisher Scientific) and imaged using a Chemidoc (Biorad).

Macrophage infection with *M. abscessus* strains.

THP-1 macrophages were grown at 37ºC in a 5% CO_2 incubator in RPMI 1640 supplemented with 10% FBS ($RPMI^{FBS}$) and differentiated for 48 hrs with 20 ng.mL-1 phorbol myristate acetate (PMA). Exponentially growing Mab strains were harvested and resuspended in PBS 1X. Single-cell bacteria were produced by passage through a 26.5-gauge needle (20 times) and then further filtered through a 5.0 µm filter (Merck Millipore). THP-1 cells were infected at a 2:1 (bacteria:macrophage) Multiplicity of Infection (M.O.I.) and grown at 37ºC in the presence of 5% CO_2. After 4 hrs incubation, cells were washed thrice with PBS 1X and incubated with $RPMI^{FBS}$ supplemented with 250 µg.mL^{-1} AMK for 2 hrs to eliminate extracellular bacilli. Infected THP-1 macrophages were cultured in $RPMI^{FBS}$ supplemented with AMK maintained at 50 µg.mL^{-1}.

Bacterial extracellular growth was prevented by refreshing the culture medium containing AMK 50 µg.mL^{-1} every two days. Before plating the bacteria, THP-1 macrophages were washed thrice with PBS 1X. Cell lysis was achieved with 100 µL of 1% Triton X100 in PBS 1X. Then, 900 µl of 1x PBS was added to each well and ten-fold dilutions were plated onto LB agar. This procedure was repeated at 0, 1, 3 and 5 days post-infection. After 5 days of incubation at 37ºC, the number of CFU was assessed. The CFUs counts were plotted on a logarithmic scale and the standard error bars were calculated using the GraphPad Prism software.

Growth curves of *M. abscessus* strains

Cultures of 20 mL were inoculated with single-cell preparations in 7H9^{OADC} supplemented with 0.025% tyloxapol (starting OD_{600nm} of 0.05) and incubated at 37ºC under agitation (100 rpm) for 5 days. The OD was monitored daily. The OD values were plotted and error bars were calculated using the GraphPad Prism software.

Drug susceptibility testing

The minimal inhibitory concentration (MIC) experiments were determined for the following antibiotics: bedaquiline, cefoxitin, ethambutol, vancomycin, ciprofloxacin, imipenem, kanamycin B, hygromycin B, amikacin, tigecycline and clofazimine. MICs were determined according to the Clinical and Laboratory Standards Institute (CLSI) guidelines [37]. The broth microdilution method was used in Cation-adjusted Mueller-Hinton broth (CaMHB) with single-cell preparations of Mab wild-type, Δ*MAB_4324c* and corresponding to 5 × 10^6 CFU.mL^{-1}. Serial dilutions of the drug (100 µL) were added to 100 µL of bacterial suspension and incubated for 3-5 days at 30ºC.

Results and Discussion

MAB_4324c is an active *N*-acetyltransferase

Sequence analysis of MAB_4324c using the Pfam server [38] predicted the presence of a well-conserved GNAT domain in its C-terminus as well as a second GNAT domain displaying lower conservation in its N-terminus. This analysis indicates that MAB_4324c may belong to the tandem repeat *N*-acetyltransferase family. MAB_4324c shares a low protein sequence identity with the well-characterized Eis proteins and does not possess the same modular organization.

To inquire whether MAB_4324c possesses *N*-acetyltransferase activity, we performed a biochemical analysis of the protein. First, MAB_4324c was recombinantly expressed in *E. coli* and the soluble protein was subsequently purified following a three-step purification procedure. Highly pure MAB_4324c preparations were obtained **(Fig.1 A)** and assessed for molecular weight

determination by size-exclusion chromatography (SEC) **(Fig.1 A)**. The protein was eluted at a volume of 14.5 mL using a Superdex 200 10/300 GL Increase column. This elution profile corresponds to an apparent molecular weight of 42.6 kDa, which is in line with the theoretical mass of 39.1 kDa. This indicates that the protein is a monomer in solution.

We next assessed the activity of MAB_4324c with a few substrates known as substrates of *N*-acetyltransferases belonging to different classes [39,40]. *N*-acetyltransferases substrates are highly diverse and, without any closely related protein whose function is known it was difficult to determine the substrate of MAB_4324c. As the Eis members of the GNAT protein in mycobacteria can modify aminoglycosides through acetylation of their primary amines, we first tested if MAB_4324c could modify this class of antibiotics. The near absence of or very low activity could be noticed using APR, HYG or AMK as substrates and ACO as a cofactor **(Fig.1 B)**. We next tested substrates suited for numerous GNAT and all possessing primary amines notably histamine, tyramine, spermine and spermidine **(Fig.1 B)** [14,40]. This screening identified only spermine and spermidine as substrates of MAB_4324c, with a slightly better apparent activity for spermidine **(Fig.1 B)**. To ensure that the reaction we observed was enzyme-specific, additional control experiments were performed with the heat-inactivated enzyme or with reactions lacking either the enzyme or the cofactor. As expected, the *N*-acetyltransferase activity was only detected in the presence of a functional MAB_4324c **(Fig. S1A)**. The kinetic parameters of MAB_4324c for spermidine and acetyl-CoA were determined **(Table I) (Fig. 1C, 1D and S1B, S1C)**. The relatively low catalytic efficiency and very low K_M suggest that spermidine is not the cognate substrate of MAB_4324c though these kinetic data attest that MAB_4324c is an active *N*-acetyltransferase capable of transferring acetyl group to primary amines.

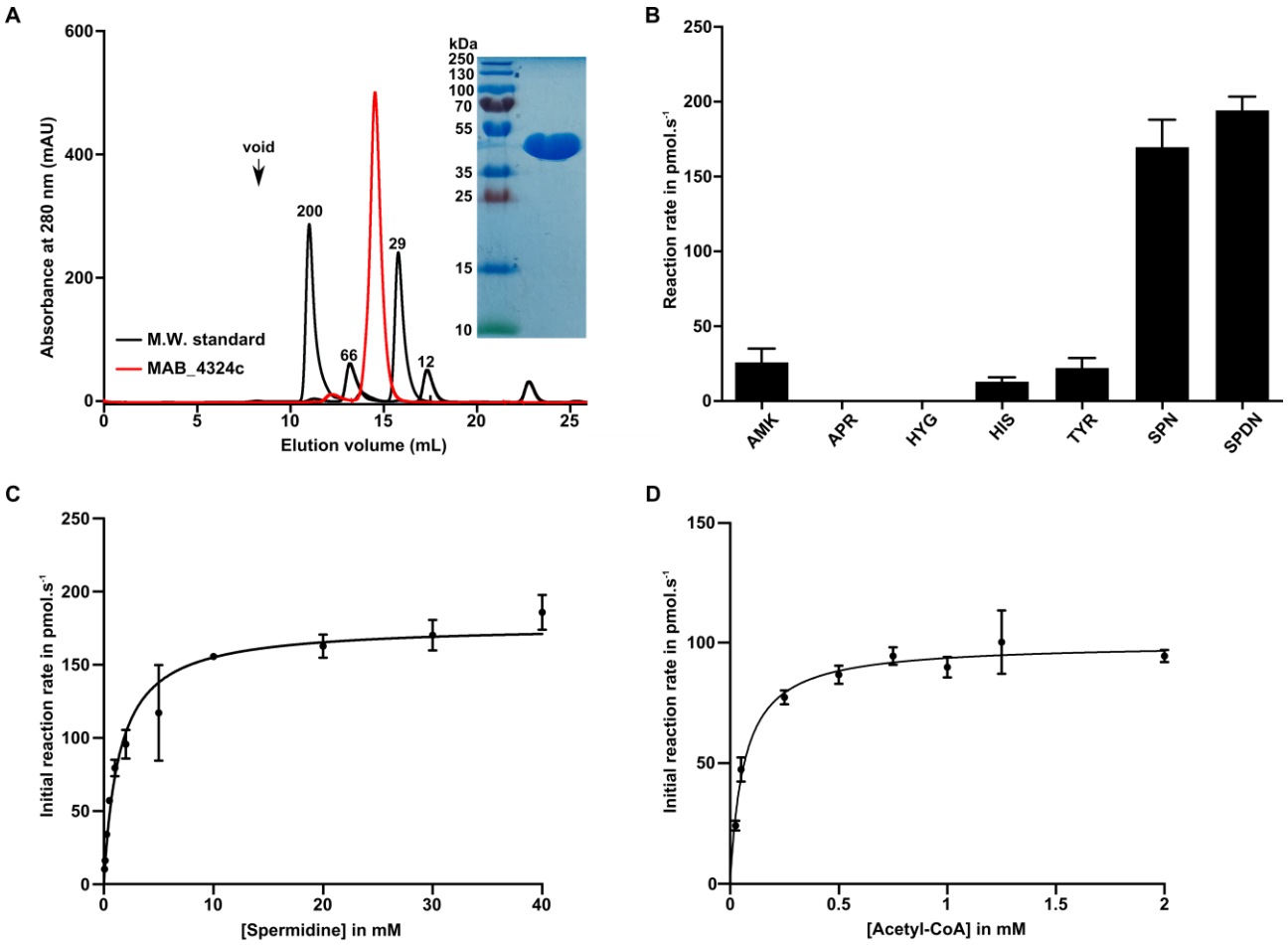

FIGURE 1

Figure 1. Biochemical characterization of MAB_4324c

(A) Coomassie Blue-stained SDS polyacrylamide gel electrophoresis attesting the purity of MAB_4324c obtained after three steps of purification (10 µg of protein were loaded on the gel). Estimation of the oligomeric state of MAB_4324c, depleted from its tags, by SEC. The elution profile of the proteins used for calibration on the Superdex 200 increase 10/300 GL column is displayed as a black line and the elution profile of MAB_4324c is indicated in red. Calibration was established using β-amylase (200 kDa), bovine serum albumin (66 kDa), carbonic anhydrase (29 kDa), and cytochrome C (12.4 kDa), eluted with estimated volumes of 11.07, 13.2, 15.8 and 17.3 mL, respectively. The void volume indicated by the black arrow was estimated at 8.3 mL with dextran blue. The MAB_4324c elution peak at 14.5 mL corresponds to an apparent molecular weight of 42.6 kDa. (B) Substrate specificity assessment of MAB_4324c. The initial rates were determined in presence of 10 mM of each of the following substrates: AMK, apramycin (APR), hygromycin B (HYG), histamine (HIS), tyramine (TYR), spermine (SPR) or spermidine (SPDN). Acetyl-CoA at 0.5 mM was used as a cofactor. (C) Michaelis-Menten curve used to determine the kinetic constants for spermidine in the presence of 0.5 mM of acetyl-CoA. (D) Michaelis-Menten curve was used to determine the kinetic constants for acetyl-CoA in the presence of 40 mM spermidine.

Table I. Kinetic parameters of MAB_4324c.

Substrates	V_{max} (pmol.s^{-1})	K_M (µM)	k_{cat} (s^{-1})	K_M/k_{cat} (M^{-1} s^{-1})
Acetyl-CoA	99.6 ± 0.02	63 ± 0.07	0.39 x 10^{-3} ±0.008	0.16
Spermidine	186.4 ±5	1.66 x 10^{3} ±0.22	0.74 x 10^{-3} ±3.8 10^{-5}	2.24

MAB_4324c is a tandem repeat *N*-acetyltransferase

To support the biochemical data, we engaged in structural studies of MAB_4324c. We succeeded in obtaining exploitable crystals of the protein when it was co-crystallized with acetyl-CoA. Structure phasing was achieved through the sulfur-single-wavelength anomalous dispersion method **(Table II)**.

The partial model built thanks to the anomalous map was further used to solve the structure obtained from a 2Å resolution native dataset.

Two monomers occupy the asymmetric unit **(Fig. 2A)**. Most of the residues could be rebuilt for the two monomers except for the first 11 and 12 residues of our expressed construct (that contains one extra Gly residue coming from the TEV cleavage site on top of the MAB_4324c sequence) in monomers A and B respectively. We could not build some residues of the loop between strands 8 and 9 due to very poor electron density in this area.

Crystal packing analysis did not argue in favor of a functional dimer and, in agreement with the oligomeric state of the protein observed by SEC **(Fig. 1A)**. The MAB_4324c overall structure **(Fig. 2B)** is composed of 12 β-strands and 11 α-helices forming two GNAT domains interconnected to each other with two β-strands (β6 and β12). The structure can be divided into two major subdomains: domain 1 in the N-terminus is containing residues 1-177 (α1-α6 and β1-β6) and is a GNAT domain although the e-value ($8.4x10^{-5}$) for this signature motif is quite low when analyzed at the Pfam server. Domain 2 in the C-terminus encompasses residues 178-352 (α7-α11 and β7-β12) and matches a GNAT domain signature with a much better score (e-value=$3.9x10^{-11}$) than domain 1. These two domains share 13% sequence identity and their superposition based on their secondary structure and over the main chain of 137 residues led to a r.m.s.d. value of 2.1Å (not shown), attesting to a certain degree of structural divergence but not as high as it would have been expected based on the sequence homology.

The two monomers from the asymmetric unit are not equivalent in terms of ligand binding **(Fig. 2A)**. The two C-terminal subdomains bind acetyl-CoA (**Fig. 2A and 3A)**. This ligand is in fact in two forms as an acetyl-CoA and as another one where acetyl-CoA is cleaved into CoA and acetate. All ligand occupancies were estimated to be 0.5 **(Fig. S2)**. Unexpectedly, a ligand neither corresponding to acetyl-CoA nor CoA was bound to domain 1 in each of the two monomers of the asymmetric unit. The clear simulated annealed omit maps [41] allowed without ambiguity the identification of NADH in one monomer and NADPH in the second one **(Fig. 3B)**. In one monomer of the asymmetric unit, NADH could be placed however in the other monomer, NADPH was modelled. Since none of these ligands were added exogenously during the crystallization process, it appears obvious that they were co-purified during the purification of MAB_4324c. Of note, NADPH was not modelled in both chains as the phosphate group cannot pack due to steric

hindrance with the symmetry mate (not shown) in chain B and electron density does not support the presence of the additional phosphate group **(Fig. 3B)**.

Table II. X-ray data collection and refinement statistics.

	MAB_4324c native	MAB_4324c Sulfur SAD
Wavelength (Å)	1	2.08
Resolution range (Å)	49.09 -2.0 (2.072-2.0)	49.26 - 2.33 (2.39 - 2.33)
Space group	*P* 65 2 2	*P* 65 2 2
Unit cell (Å,°)	149.96 149.96 183.38, 90 90 120	150.49 150.49 184.14, 90 90 120
Total reflections	3143788 (302942)	19074956 (230331)
Unique reflections	82207 (8058)	99388 (7401)
Multiplicity	38.2 (37.6)	191.9 (31.1)
Completeness (%)	96.84 (99.98)	99.00 (99.30)
Mean I/sigma(I)	39.58 (5.79)	32.18 (0.82)
Wilson *B*-factor (Å^2)	26.2	48.55
***R*-meas**	0.115 (0.87)	0.278 (4.43)
CC1/2	1 (0.95)	1 (0.45)
Reflections used in refinement	79620 (8058)	
Reflections used for *R*-free	1969 (199)	
***R*-work**	0.186 (0.183)	
***R*-free**	0.225 (0.236)	
Number of non-hydrogen atoms	6620	
macromolecules	5437	
ligands	340	
solvent	860	
Protein residues	679	
RMS (bonds, Å)	0.01	
RMS (angles, °)	1	
Ramachandran favored (%)	98.66	
Ramachandran allowed (%)	1.34	
Ramachandran outliers (%)	0	
Rotamer outliers (%)	0.36	
Clash score	3.6	
Average *B*-factor (Å^2)	31.5	
macromolecules	29.9	
ligands	37.9	
solvent	39.3	

Values between parentheses are for the last resolution shell.

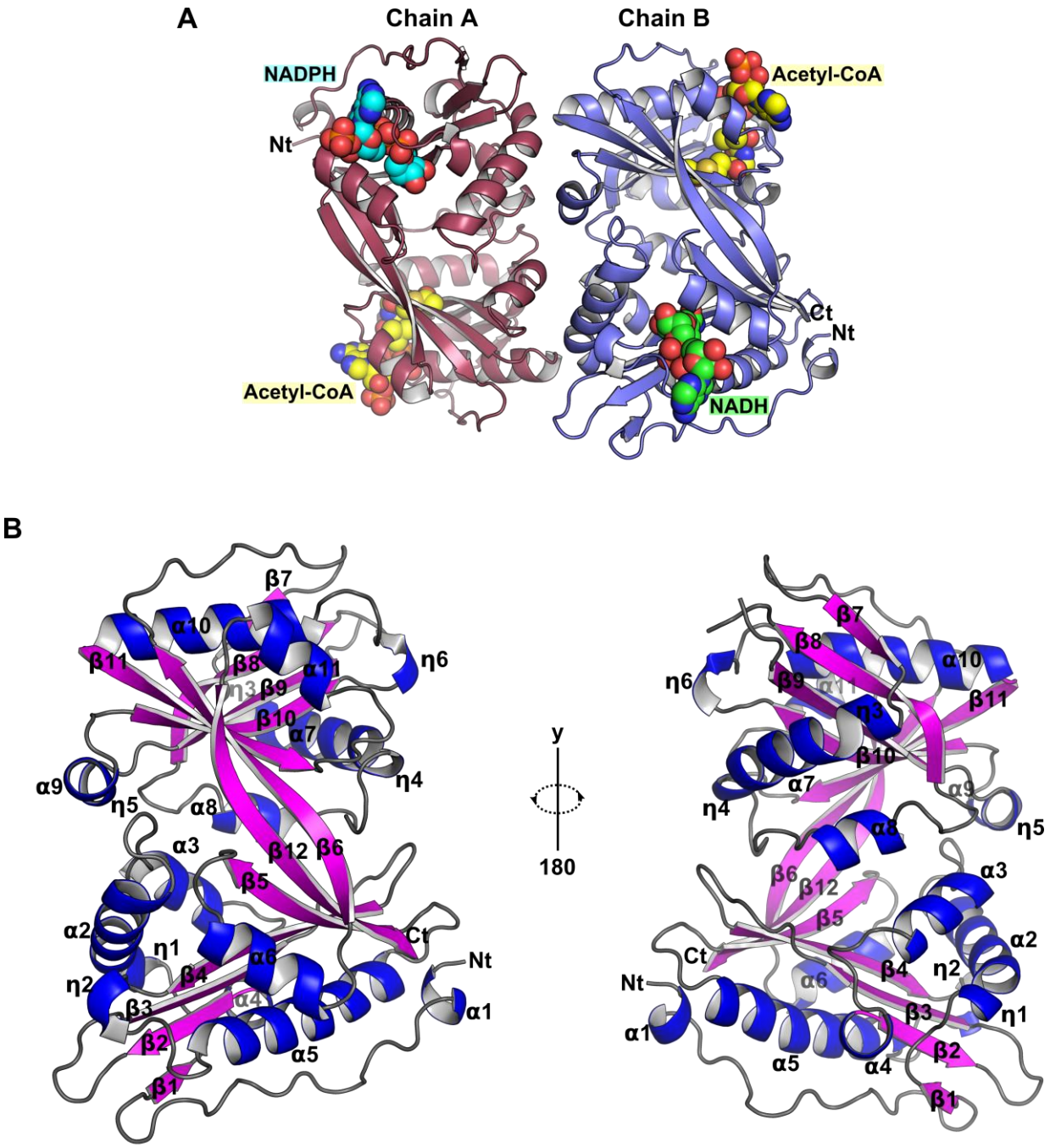

FIGURE 2

Figure 2. Overall crystal structure of MAB_4324c

(A) Composition of the asymmetric unit (A.U). Two non-equivalent monomers of MAB_4324c occupy the A.U. The two monomers are similar with the exception that the N-terminal subdomain of chain A binds NADPH while NADH is present in the N-terminal subdomain of chain B. Nt and Ct stand for N-terminus and C-terminus respectively. (B) Overall structure of MAB_4324c. Alpha (α) and 3_{10} (η) helices appear as blue cartoons while beta-strands (β) are colored in pink. Loops or coils are in grey.

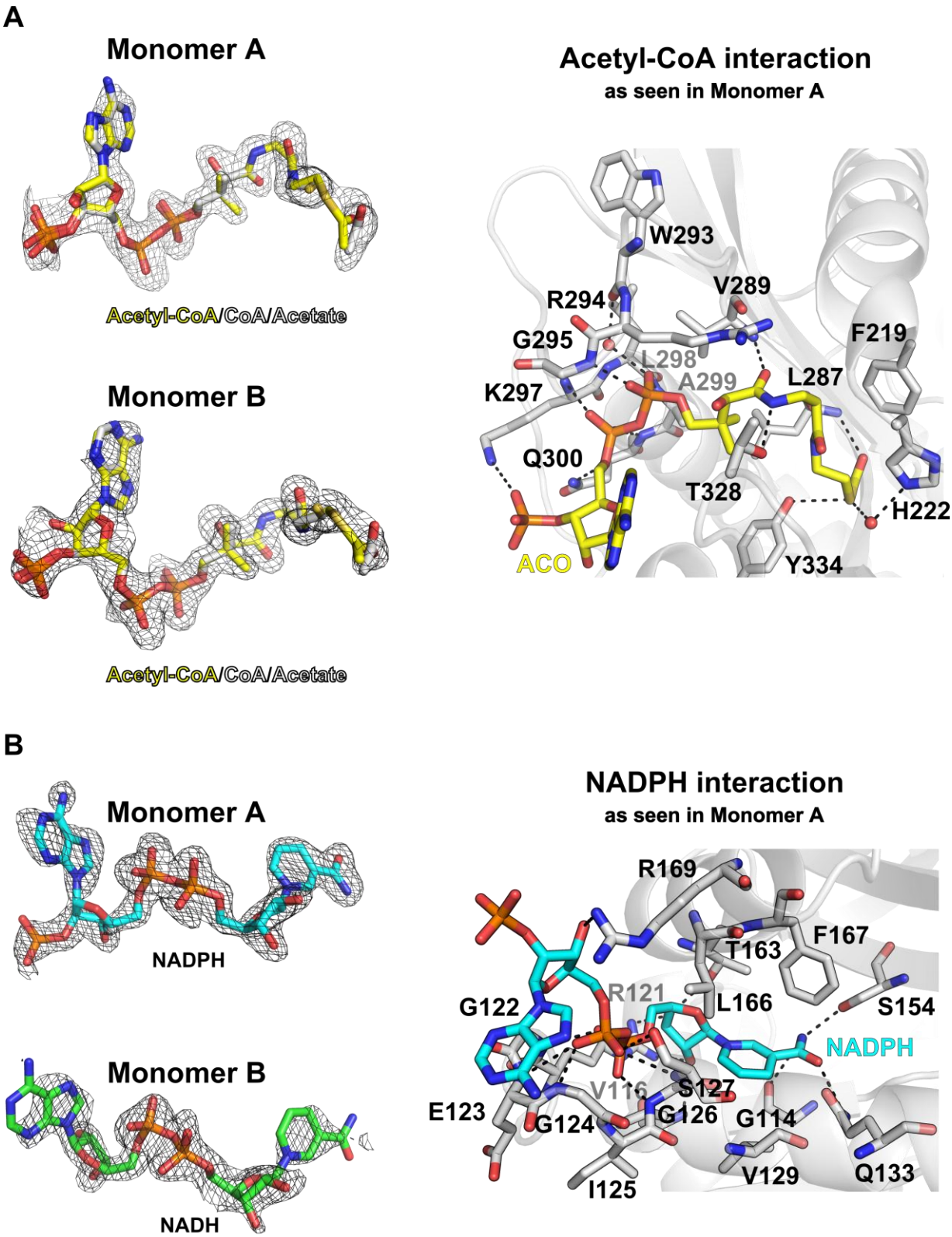
A
Monomer A
Acetyl-CoA/CoA/Acetate
Monomer B
Acetyl-CoA/CoA/Acetate
Acetyl-CoA interaction
as seen in Monomer A
W293
V289
R294
G295
L298
A299
L287
F219
K297
Q300
T328
H222
ACO
Y334
B
Monomer A
NADPH
Monomer B
NADH
NADPH interaction
as seen in Monomer A
R169
F167
T163
R121
L166
S154
G122
NADPH
V116
S127
E123
G124
G126
G114
V129
Q133
I125

FIGURE 3

Figure 3. Acetyl-CoA and NADH/NADPH recognition by MAB_4324c

(A) Recognition of acetyl-CoA. The simulated-annealed omit maps contoured at the 3 sigma level are displayed for acetyl-CoA/CoA/acetate as seen in chains A and B. The acetyl-CoA (yellow sticks) and CoA/acetate group (white stick) were refined to an occupancy of about 0.5 each (left panels). On the right panel are displayed the interactions between the cofactor and the MAB_4324c active site residues as seen in chain A. Hydrogen bonds are represented by the dashed lines and water molecules are seen as red spheres. Nitrogen, oxygen and phosphate atoms are in blue, red and orange, respectively, while carbon atoms are in grey for MAB_4324c amino acids or yellow for acetyl-CoA. (B) Recognition of NADH/NADPH. The simulated-annealed omit maps contoured at the 3 sigma level are displayed for NADH/NADPH as seen in chains A and B (left panels). The right panel shows the interactions occurring between NADPH and the residues side-chains of MAB_4324c as seen in chain A. The recognition of NADH is equivalent to the one of NADPH and is, therefore, not displayed.

To ensure that NADH and NADPH are the bound forms rather than their oxidized forms and to assess to which extent MAB_4324c is bound to nicotinamide after purification, we performed a UV spectrum of the concentrated protein. In addition to the protein absorption peak at 280 nm, a second peak was detected at 340 nm and corresponding to NADH/NADPH **(Fig. S3)**. The concentration of the NADH/NADPH in the sample was estimated to 70 µM, which corresponds to the MAB_4324c concentration, indicating that the protein is saturated with the reduced forms of the nicotinamide groups since the oxidized NAD+/NADP+ forms do not display absorption peak at 340 nm.

Acetyl-CoA (ACO) is recognized by twelve residues **(Fig. 3A and Fig. 4)**, of which the side chain of H222 establishes a H-bond via one water molecule with the S atom of ACO. The sulfur is also contacted by the Y334 side chain. H222 and Y334 interact with the ACO S-group and thus are very likely to be important catalytic residues. This is particularly true for Y334 as it was already proposed that the side chain of the catalytic Y residue of the RimI acetyltransferase might be important as a general acid for the protonation of the ACO sulfhydryl group before the transfer of the acetyl group [42,43]. F219 interacts by hydrophobic interaction with the acetyl moiety that is also stabilized by the main chain of L287. The main chains of T328 and V289 form a H-bond with the NH and CO groups of the pantothenate. The phosphates of ADP are interacting with the main chains of W293 (via one water molecule), G295, Q300 and K297, while the latter also binds the phosphate of the ACO ribose with its side chain. Finally, the side chain of R294 stacks the ACO.

Recognition of NADPH involves a complex network of interactions **(Fig. 3B and Fig. 4)**. The nicotinamide group of NADPH is contacted by the side chains of Q133 and S154 as well as by the main chain of G114. F167, V129 and L166 mediate van der Waals interactions with the nicotinamide group. The hydroxyl of the ribose is contacted via H-bonds by the side chains of R121, T163 and the main chain of V116. The main chain of G122, E123, G124 and G126 tightly bind to the phosphate group of ADP moiety. The last interaction involves the side chain of R169 that establishes a H-bond with the ribose of the ADP.

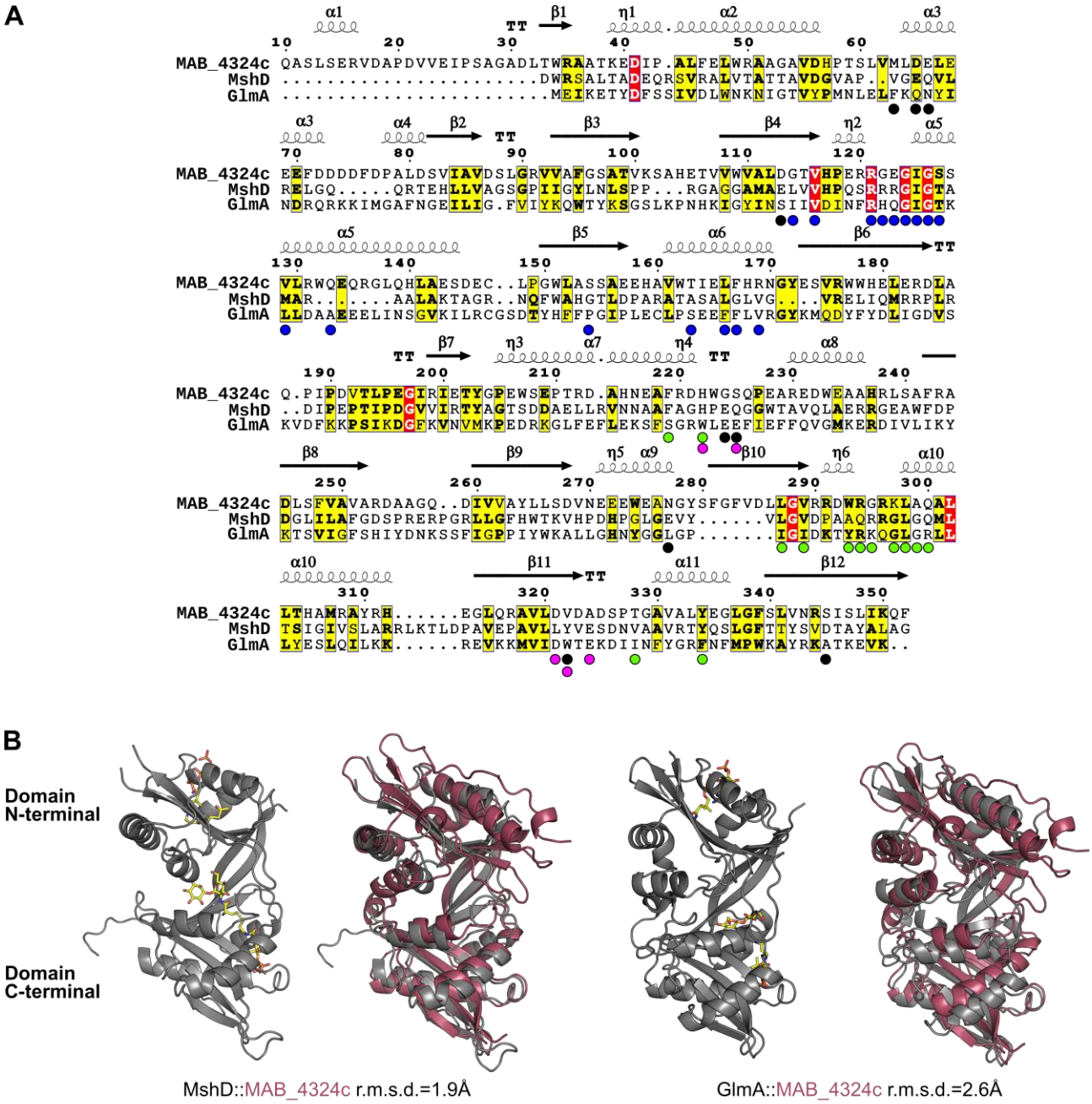

FIGURE 4

Figure 4. Comparison of MAB_4324c with structural homologues

(A) Multiple sequence alignment was performed with ENDscript [55] and adjusted manually with the Inkscape software. The secondary structure (α, α-helix, β, β-strand, η, 3_{10}-helix) of MAB_4324c obtained from its crystal structure, is indicated above the alignment. Residues involved in NADPH and ACO binding in MAB_4324c are indicated by the blue and green circles, respectively. The pink and black circles indicate the amino acids involved in carbohydrate binding in the Glucosamine/Glucosaminide N-acetyltransferase, GlmA (PDB id: 5KGP) and the mycothiol synthase MshD (PDB id: 2C27) crystal structures. (B) Superposition of the MshD and GlmA (both as a grey cartoon) onto the MAB_4324c (raspberry cartoon) crystal structure. The substrates bound to MshD and GlmA are shown as yellow sticks. The r.m.s.d. values are reported below each structural alignment.

The identification of a binding site for nicotinamide is particularly intriguing since, to our knowledge, GNAT domains have never been reported to bind to NADH/NADPH. It is well documented however that the type III GNAT enzymes are allosterically regulated by metabolic compounds [44]. This is the case for the GNAT enzyme (Rv0998) from *M. tuberculosis* which is allosterically regulated by cyclic AMP (cAMP) [45]. Activation of the enzyme's activity occurs upon binding of cAMP that triggers a large conformational switch. However, the GNAT domain is not the domain that binds cAMP [46]. The *N*-acetyltransferase MxKat from *Myxococcus xanthus* can bind to NADP+ thanks to its N-terminal domain consisting of a Rossmann fold and binding to NADP+ which inhibits the enzyme activity [47]. To assess if NADH or NADPH could play a role in regulating or modulating the enzymatic activity of MAB_4324c, we compared the kinetic constants of MAB_4324c for spermidine and in presence of 0.1 mM of the reduced nicotinamide forms. The enzymatic properties were however not significantly affected by the addition of NADH or NADPH **(Fig. S4 and Table S1)**. Interestingly, it was also proposed that the *N*-terminal GNAT domain of the mycothiol synthase is not catalytically active but its capacity to bind CoA may assist the enzyme to fold [48] suggesting that NADH or NADPH may be helpful for the folding of MAB_4324c.

We then attempted to search for MAB_4324c structural homologues whose biological function or enzymatic function was elucidated. This led to the identification of only two related structures **(Fig. 4)**: the mycothiol synthase from *Mycobacterium tuberculosis* (PDB id: 2C27) [48] bound to des-acetylmycothiol and CoA that possesses a r.m.s.d. of 1.9Å and sequence identity of 19%, and the structure of glucosamine *N*-acetyltransferase bound to chitosan, GlmA, from *Clostridium acetobutylicum* (PDB id : 5kgp) sharing a r.m.s.d. of 2.6 Å and sequence identity of 12% [49]. These two enzymes are also tandem repeat *N*-acetyltransferases but are involved in different pathways. MshD is an essential enzyme for mycobacteria as it catalyzes the last step of mycothiol synthesis, a key component in protection against oxidative stress. Mycothiol is made of an acetylated Cys residue, a glucosamine residue, and an inositol group. GlmA ensures the transfer of an acetyl group from ACO to the amino group of glucosamine [50] and seems to be involved in cell wall recycling. These three enzymes have in common the ability to bind ACO and indeed residues involved in ACO binding are well conserved in the three proteins **(Fig. 4)**. In the MshD structure, glucosamine is tightly bound by V34, E36, Q37, E79, E179, Q180, E234, Y282 and D305 [48]. In GlmA W193, E196, D287, W288 and E290 are key residues for carbohydrate-binding [49]. Only a few of the residues involved in carbohydrate binding in these two enzymes are however conserved in MAB_4324c, suggesting a different function for the latter **(Fig. 4)**.

The fact that MAB_4324c could be the mycothiol synthase in Mab cannot be excluded. A BLAST search using MshD (Rv0819) retrieves MAB_0745 as the closest homologue of the mycothiol synthase, sharing 51% sequence identity and 61% similarity. A strong experimental

argument for excluding MAB_4324c as the main mycothiol synthase relies on the fact that, while the mycothiol synthase is an essential enzyme in mycobacteria, we were able to generate a MAB_4324c deletion mutant in Mab, as shown below **(Fig. 5)**. While this suggests that MAB_4324c is unlikely to be a mycothiol synthase, we cannot rule out a redundant or closely related function that is not essential for Mab.

Nevertheless, the structural analysis attesting strong structural proximity with proteins involved in carbohydrate metabolism/synthetic pathway underlines the possibility that MAB_4324c may participate in the acetylation of substrates possessing a carbohydrate moiety, which remains to be discovered.

Closely related MAB_4324c homologues are mainly found in actinobacteria

We searched for the presence of MAB_4324c orthologues in other mycobacterial species, but none of them were identified in *Mycobacterium leprae*, *Mycobacterium smegmatis*, *M. tuberculosis*, or *Mycobacterium marinum*. However, additional searches using the HMMER server identified very closely related homologues in numerous bacteria, mainly within the actinobacteria phylum. Multiple sequence alignments of the best hits highlight a high conservation level with MAB_4324c **(Fig. S5)**. Highly conserved protein sequences were found within the *M. abscessus* complex including subspecies *M. bolletii*, and *M. massiliense* and one orthologue was found in the phylogenetically related *Mycobacterium chelonae*. Other occurrences were found in other mycobacteria, such as *Mycobacterium immunogenum* or *Mycobacterium wolinskyi* and other actinobacteria of the Streptomycetaceae, Microbacteriaceae groups as well as in a few Proteobacteria from the Burkholderiales group. This analysis indicates that the protein is not conserved necessarily in pathogenic bacteria but rather in environmental bacteria.

***MAB_4324c* is dispensable for *M. abscessus* planktonic growth**

To investigate the role of *MAB_4324c*, a deletion mutant was generated by the use of a homologous recombination technique enabling the production of unmarked deletion mutants in Mab **(Fig. 5A)** [9]. Gene deletion was obtained in the Mab smooth background. The gene deletion was confirmed by PCR genotyping and sequencing **(Fig. 5B)**. Complementation of the deletion strain was obtained by cloning *MAB_4324c* into the episomal pMV261 [51] yielding pMV261::*MAB_4324c*. The same construct was used for overexpressing the protein in the WT background. A Strep-tag coding sequence was added in the 5'-end of the gene to monitor the protein expression by Western blotting. MAB_4324c expression was indeed detected in both WT and mutant strains **(Fig. S6)**. All strains grew similarly to the WT progenitor, suggesting that the

inactivation of MAB_4324c does not affect the planktonic growth of Mab **(Fig. 5C)**. The results indicate that *MAB_4324c* is dispensable for Mab growth in planktonic culture.

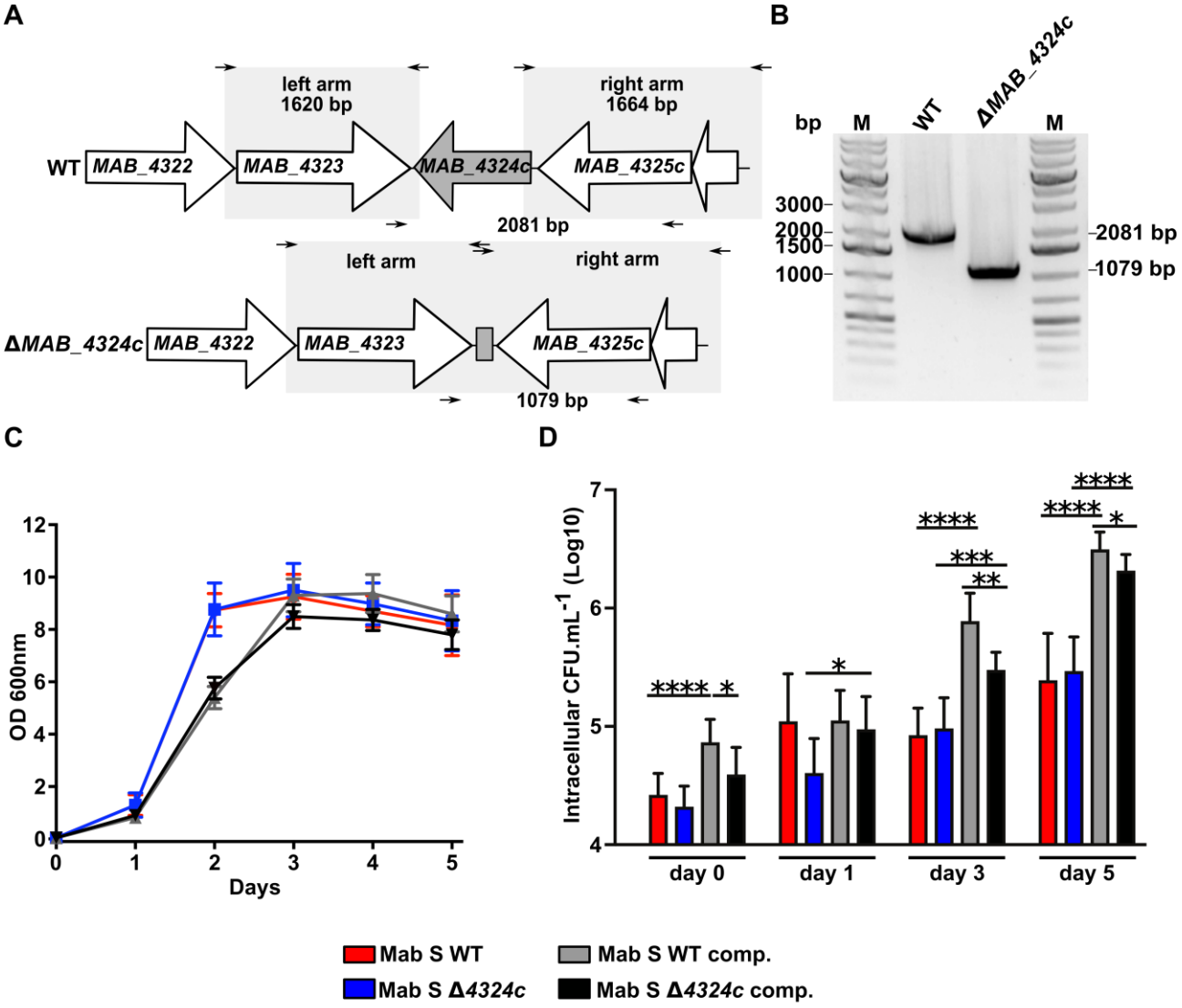

FIGURE 5

Figure 5. Generation and phenotypic analyses of ΔMAB_4324c

*(A) Genomic region of MAB_4324c in the parental (WT) and deletion (ΔMAB_4324c) strains is indicated. The size of the PCR amplicons used to genotype the ΔMAB_4324c mutant is represented. (B) PCR genotyping demonstrates the proper deletion of the mutant strain. The PCR product of 1079 pb was amplified from ΔMAB_4324c genomic DNA while a band at 2081 pb was obtained for the WT strain. (C) In vitro growth curves in liquid culture and at 37°C of the WT smooth (Mab S WT), ΔMAB_4324c (Mab S Δ4324c), complemented strains (Mab S Δ4324c comp.) as well as the WT strain overexpressing MAB_4324c (Mab S WT comp.). Experiments were performed in triplicates. (D) Infection of THP-1 macrophages with Mab. Histograms and error bars represent the means and standard deviations calculated from three independent experiments. For statistical analysis, the unpaired t-test with Welch's correction was applied. *, **, *** and **** stands for p<0.05, p<0.005, p<0.001 and p<0.0001, respectively.*

MAB_4324c does not trigger resistance to clinically relevant drugs

Transcriptomic data attested that *MAB_4324c* expression is controlled by the transcriptional WhiB7 regulator [15]. Upon stress responses, WhiB7 upregulates the expression of numerous genes and particularly those involved in antibiotic resistance. It was notably shown that the expression of the *N*-acetyltransferase $Eis2_{Mab}$ that inactivates amikacin [13], is indeed controlled by WhiB7 [15]. Further, RNAseq analysis revealed that *MAB_4324c* among other genes is upregulated upon exposure of Mab to several classes of antibiotics. *MAB_4324c* is upregulated upon exposure to clinically relevant antibiotics such as amikacin, clarithromycin and tigecycline [24]. We thus, tested whether *MAB_4324c* contributes to antibiotic resistance in Mab. To do so, MICs of a limited set of antibiotics were determined in Δ*MAB_4324c* and compared with those of the WT strain. However, no major differences were noticed in the drug susceptibility profile between the two strains **(Table S2)**. Albeit, while we only tested a limited number of antibiotics, this study suggests that, in contrast to $Eis2_{Mab}$, MAB_4324c is unlikely to play a role in drug resistance mechanisms in Mab.

MAB_4324c is not involved in protein acetylation

Lysine acetylation is a ubiquitous posttranslational modification in bacteria [44] and this is particularly true in mycobacteria. In *M. tuberculosis* about 140 proteins involved in numerous metabolic processes were shown to be acetylated [52]. We thus addressed the possibility that MAB_4324c participates in protein acetylation. We compared the acetylome of the WT, Δ*MAB_4324c* and the corresponding MAB_4324c-overexpressing strains by Western blotting using a pan anti-acetylated lysine primary antibody. No major differences were observed when comparing the acetylome of the four strains, suggesting that MAB_4324c cannot acetylate proteins **(Fig. S7)**. However, more sensitive assays, such as acetylated peptide enrichment coupled to mass spectrometry, are required to support this hypothesis. Additionally, it would be relevant to explore whether MAB_4324c acetylates host proteins, although this is very unlikely given the fact that MAB_4324c is not predicted to be secreted.

MAB_4324c overexpression confers intracellular survival in human macrophages

A recent RNAseq study identified a set of genes that are specifically upregulated during the intramacrophage growth of *M. abscessus* subspecies *massiliense* [19]. *MYCMA_RS02565* which is the orthologue of *MAB_4324c* in *M. massiliense*, was four-time more expressed under the intracellular conditions as compared to *in vitro* growth conditions. This prompted us to assess whether *MAB_4324c* plays a role in the intracellular uptake and/or survival in macrophages. On day 0, the uptake of Δ*MAB_4324c* was not affected as compared to the WT strain, however the *MAB_4324c* overexpressing strain showed increased internalization by macrophages, as determined

by the CFU counts **(Fig. 5D)**. Similarly, while Δ*MAB_4324c* failed to show alterations in intracellular survival as compared to the WT strains, infections with either the complemented strain or the WT strain overproducing *MAB_4324c* were associated with higher bacterial loads **(Fig. 5D)**. This suggests that overexpression of *MAB_4324c* provides an intracellular growth advantage with an enhanced intracellular survival capacity.

While we established that *MAB_4324c* is an active *N*-acetyltransferase, the lack of data regarding its genuine substrate makes it difficult to propose a clear function. Nonetheless, the capacity of MAB_4324c to bind NADH/NADPH might explain the phenotype observed when overexpressing MAB_4324c in Mab during macrophage infection. Supporting this hypothesis, several bacterial pathogens have developed strategies to reduce the intracellular pool of NAD+, subsequently reducing the capacity of the cell to fight against the pathogen and therefore, thus favoring escape and intracellular survival of the bacteria [53]. Of particular interest, it has been shown that Sirtuin 3 a mitochondrial deacetylase, whose function is dependent on the NAD+ pool, enhances host defense against Mab infection [54]. Thus, by sequestering nicotinamide and diminishing the concentration of NAD+ inside the host cell, MAB_4324c may reduce the host defense and facilitate the persistence of Mab inside macrophages. Another hypothesis somewhat related to the above one would be that MAB_4324c by binding NADH/NADPH controls the metabolic state of this important cofactor which might be needed to convert its planktonic to an intracellular lifestyle. However, a clear demonstration of these different proposed hypotheses awaits further experimentation.

Conflict of interest statement

The authors declare no conflict of interest.

Acknowledgments

We thank the staff at SLS beamlines for support during data collection. Funding for this work was supported by the Fondation pour la Recherche Médicale (FRM) [grant number DEQ20150331719 to LK] and, the Lundbeck Foundation, Denmark (R303-2018-2964 to HA). KLU Ph.D. fellowship was supported by the National Research Agency [ANR-17-CE11-0008-01 – MyTraM to MB]. M.D.J. received a postdoctoral fellowship granted by Labex EpiGenMed, an “Investissements d’Avenir” program (ANR-10-LABX-12-01). We would like to thank Dr. W. Daher for his help with macrophage preparations. We thank Dr J. Wong for the critical reading of the manuscript.

Author contributions

HA, KLU, JD and MB performed experiments. MB designed research. VO performed sulfur-SAD phasing. MDJ assisted with macrophage experiments. LK and MB supervised the research. MB wrote the first draft with the input of all the authors.

Data availability

The data that support the findings of this study are available from the corresponding author mickael.blaise@irim.cnrs.fr upon reasonable request. The structural data that support these findings are openly available in the wwPDB at https://doi.org/10.2210/pdb7Q3A/pdb.

Bibliography

1. Johansen MD, Herrmann JL, Kremer L. Non-tuberculous mycobacteria and the rise of Mycobacterium abscessus. *Nat Rev Microbiol*. 2020;18(7):392-407. doi:10.1038/s41579-020-0331-1
2. Bryant JM, Grogono DM, Rodriguez-Rincon D, et al. Emergence and spread of a human-transmissible multidrug-resistant nontuberculous mycobacterium. *Science*. 2016;354(6313):751-757. doi:10.1126/science.aaf8156
3. Bryant JM, Brown KP, Burbaud S, et al. Stepwise pathogenic evolution of Mycobacterium abscessus. *Science*. 2021;372(6541):eabb8699. doi:10.1126/science.abb8699
4. Ruis C, Bryant JM, Bell SC, et al. Dissemination of Mycobacterium abscessus via global transmission networks. *Nat Microbiol*. Published online September 20, 2021. doi:10.1038/s41564-021-00963-3
5. Lee MR, Sheng WH, Hung CC, Yu CJ, Lee LN, Hsueh PR. Mycobacterium abscessus Complex Infections in Humans. *Emerg Infect Dis*. 2015;21(9):1638-1646. doi:10.3201/2109.141634
6. Floto RA, Olivier KN, Saiman L, et al. US Cystic Fibrosis Foundation and European Cystic Fibrosis Society consensus recommendations for the management of non-tuberculous mycobacteria in individuals with cystic fibrosis. *Thorax*. 2016;71(Suppl 1):i1-i22. doi:10.1136/thoraxjnl-2015-207360
7. Luthra S, Rominski A, Sander P. The Role of Antibiotic-Target-Modifying and Antibiotic-Modifying Enzymes in Mycobacterium abscessus Drug Resistance. *Front Microbiol*. 2018;9:2179. doi:10.3389/fmicb.2018.02179
8. Richard M, Gutiérrez AV, Viljoen AJ, Ghigo E, Blaise M, Kremer L. Mechanistic and Structural Insights Into the Unique TetR-Dependent Regulation of a Drug Efflux Pump in Mycobacterium abscessus. *Front Microbiol*. 2018;9:649. doi:10.3389/fmicb.2018.00649
9. Richard M, Gutiérrez AV, Viljoen A, et al. Mutations in the MAB_2299c TetR regulator confer cross-resistance to clofazimine and bedaquiline in *Mycobacterium abscessus*. *Antimicrob Agents Chemother*. Published online October 15, 2018. doi:10.1128/AAC.01316-18
10. Dubée V, Bernut A, Cortes M, et al. β-Lactamase inhibition by avibactam in Mycobacterium abscessus. *J Antimicrob Chemother*. 2015;70(4):1051-1058. doi:10.1093/jac/dku510
11. Dal Molin MD, Gut M, Rominski A, Haldimann K, Becker K, Sander P. Molecular Mechanisms of Intrinsic Streptomycin Resistance in Mycobacterium abscessus. *Antimicrob Agents Chemother*. 2018;62(1):e01427-17. doi:10.1128/AAC.01427-17
12. Rominski A, Selchow P, Becker K, Brülle JK, Dal Molin M, Sander P. Elucidation of Mycobacterium abscessus aminoglycoside and capreomycin resistance by targeted deletion of three putative resistance genes. *J Antimicrob Chemother*. 2017;72(8):2191-2200. doi:10.1093/jac/dkx125

13. Ung KL, Alsarraf HMAB, Olieric V, Kremer L, Blaise M. Crystal structure of the aminoglycosides N-acetyltransferase Eis2 from Mycobacterium abscessus. *FEBS J*. 2019;286(21):4342-4355. doi:10.1111/febs.14975
14. Ung KL, Kremer L, Blaise M. Structural analysis of the N-acetyltransferase Eis1 from Mycobacterium abscessus reveals the molecular determinants of its incapacity to modify aminoglycosides. *Proteins Struct Funct Bioinforma*. 2021;89(1):94-106. doi:https://doi.org/10.1002/prot.25997
15. Hurst-Hess K, Rudra P, Ghosh P. Mycobacterium abscessus WhiB7 Regulates a Species-Specific Repertoire of Genes To Confer Extreme Antibiotic Resistance. *Antimicrob Agents Chemother*. 2017;61(11):e01347-17. doi:10.1128/AAC.01347-17
16. Nash KA, Brown-Elliott BA, Wallace RJ Jr. A novel gene, erm(41), confers inducible macrolide resistance to clinical isolates of Mycobacterium abscessus but is absent from Mycobacterium chelonae. *Antimicrob Agents Chemother*. 2009;53(4):1367-1376. doi:10.1128/AAC.01275-08
17. Richard M, Gutiérrez AV, Kremer L. Dissecting erm(41)-Mediated Macrolide-Inducible Resistance in Mycobacterium abscessus. *Antimicrob Agents Chemother*. 2020;64(2). doi:10.1128/AAC.01879-19
18. Ripoll F, Pasek S, Schenowitz C, et al. Non mycobacterial virulence genes in the genome of the emerging pathogen Mycobacterium abscessus. *PloS One*. 2009;4(6):e5660. doi:10.1371/journal.pone.0005660
19. Dubois V, Pawlik A, Bories A, et al. Mycobacterium abscessus virulence traits unraveled by transcriptomic profiling in amoeba and macrophages. *PLoS Pathog*. 2019;15(11):e1008069. doi:10.1371/journal.ppat.1008069
20. Wei J, Dahl JL, Moulder JW, et al. Identification of a Mycobacterium tuberculosis gene that enhances mycobacterial survival in macrophages. *J Bacteriol*. 2000;182(2):377-384.
21. Duan L, Yi M, Chen J, Li S, Chen W. Mycobacterium tuberculosis EIS gene inhibits macrophage autophagy through up-regulation of IL-10 by increasing the acetylation of histone H3. *Biochem Biophys Res Commun*. 2016;473(4):1229-1234. doi:10.1016/j.bbrc.2016.04.045
22. Green KD, Biswas T, Chang C, et al. Biochemical and structural analysis of an Eis family aminoglycoside acetyltransferase from bacillus anthracis. *Biochemistry*. 2015;54(20):3197-3206. doi:10.1021/acs.biochem.5b00244
23. Chen W, Biswas T, Porter VR, Tsodikov OV, Garneau-Tsodikova S. Unusual regioversatility of acetyltransferase Eis, a cause of drug resistance in XDR-TB. *Proc Natl Acad Sci U S A*. 2011;108(24):9804-9808. doi:10.1073/pnas.1105379108
24. Schildkraut JA, Coolen JPM, Burbaud S, et al. RNA-sequencing elucidates drug-specific mechanisms of antibiotic tolerance and resistance in M. abscessus. *Antimicrob Agents Chemother*. Published online October 11, 2021:AAC0150921. doi:10.1128/AAC.01509-21
25. Henrich B, Bergamaschi A, Broennimann C, et al. PILATUS: A single photon counting pixel detector for X-ray applications. *Nucl Instrum Methods Phys Res Sect Accel Spectrometers Detect Assoc Equip*. 2009;607(1):247-249. doi:10.1016/j.nima.2009.03.200
26. Waltersperger S, Olieric V, Pradervand C, et al. PRIGo: a new multi-axis goniometer for macromolecular crystallography. *J Synchrotron Radiat*. 2015;22(4):895-900. doi:10.1107/S1600577515005354
27. Weinert T, Olieric V, Waltersperger S, et al. Fast native-SAD phasing for routine macromolecular structure determination. *Nat Methods*. 2015;12(2):131-133. doi:10.1038/nmeth.3211
28. Kabsch W. Integration, scaling, space-group assignment and post-refinement. *Acta Crystallogr D Biol Crystallogr*. 2010;66(Pt 2):133-144. doi:10.1107/S0907444909047374
29. Karplus PA, Diederichs K. Linking crystallographic model and data quality. *Science*. 2012;336(6084):1030-1033. doi:10.1126/science.1218231
30. Sheldrick GM. A short history of SHELX. *Acta Crystallogr A*. 2008;64(1):112-122. doi:10.1107/S0108767307043930

31. Usón I, Sheldrick GM. An introduction to experimental phasing of macromolecules illustrated by SHELX; new autotracing features. *Acta Crystallogr Sect Struct Biol*. 2018;74(2):106-116. doi:10.1107/S2059798317015121
32. Skubák P, Pannu NS. Automatic protein structure solution from weak X-ray data. *Nat Commun*. 2013;4:2777. doi:10.1038/ncomms3777
33. Emsley P, Lohkamp B, Scott WG, Cowtan K. Features and development of Coot. *Acta Crystallogr D Biol Crystallogr*. 2010;66(Pt 4):486-501. doi:10.1107/S0907444910007493
34. Adams PD, Afonine PV, Bunkóczi G, et al. PHENIX: a comprehensive Python-based system for macromolecular structure solution. *Acta Crystallogr D Biol Crystallogr*. 2010;66(2):213-221. doi:10.1107/S0907444909052925
35. Richard M, Gutiérrez AV, Viljoen A, et al. Mutations in the MAB_2299c TetR Regulator Confer Cross-Resistance to Clofazimine and Bedaquiline in Mycobacterium abscessus. *Antimicrob Agents Chemother*. 2019;63(1):e01316-18. doi:10.1128/AAC.01316-18
36. Stover CK, de la Cruz VF, Fuerst TR, et al. New use of BCG for recombinant vaccines. *Nature*. 1991;351(6326):456-460. doi:10.1038/351456a0
37. Woods GL, Brown-Elliott BA, Conville PS, et al. *Susceptibility Testing of Mycobacteria, Nocardiae, and Other Aerobic Actinomycetes*. 2nd ed. Clinical and Laboratory Standards Institute; 2011. Accessed October 22, 2020. http://www.ncbi.nlm.nih.gov/books/NBK544374/
38. Mistry J, Chuguransky S, Williams L, et al. Pfam: The protein families database in 2021. *Nucleic Acids Res*. 2021;49(D1):D412-D419. doi:10.1093/nar/gkaa913
39. Kuhn ML, Majorek KA, Minor W, Anderson WF. Broad-substrate screen as a tool to identify substrates for bacterial Gcn5-related N-acetyltransferases with unknown substrate specificity. *Protein Sci Publ Protein Soc*. 2013;22(2):222-230. doi:10.1002/pro.2199
40. Pan Q, Zhao FL, Ye BC. Eis, a novel family of arylalkylamine N-acetyltransferase (EC 2.3.1.87). *Sci Rep*. 2018;8(1):1-8. doi:10.1038/s41598-018-20802-6
41. Hodel A, Kim SH, Brünger AT. Model bias in macromolecular crystal structures. *Acta Crystallogr A*. 1992;48(6):851-858. doi:10.1107/S0108767392006044
42. Vetting MW, Bareich DC, Yu M, Blanchard JS. Crystal structure of RimI from Salmonella typhimurium LT2, the GNAT responsible for Nα-acetylation of ribosomal protein S18. *Protein Sci*. 2008;17(10):1781-1790. doi:10.1110/ps.035899.108
43. Christensen DG, Meyer JG, Baumgartner JT, et al. Identification of Novel Protein Lysine Acetyltransferases in Escherichia coli. *mBio*. 2018;9(5):e01905-18. doi:10.1128/mBio.01905-18
44. Lammers M. Post-translational Lysine Ac(et)ylation in Bacteria: A Biochemical, Structural, and Synthetic Biological Perspective. *Front Microbiol*. 2021;12:757179. doi:10.3389/fmicb.2021.757179
45. Nambi S, Basu N, Visweswariah SS. cAMP-regulated Protein Lysine Acetylases in Mycobacteria. *J Biol Chem*. 2010;285(32):24313-24323. doi:10.1074/jbc.M110.118398
46. Lee HJ, Lang PT, Fortune SM, Sassetti CM, Alber T. Cyclic-AMP regulation of protein lysine acetylation in Mycobacterium tuberculosis. *Nat Struct Mol Biol*. 2012;19(8):811-818. doi:10.1038/nsmb.2318
47. Liu XX, Liu WB, Ye BC. Regulation of a Protein Acetyltransferase in Myxococcus xanthus by the Coenzyme NADP. *J Bacteriol*. 2015;198(4):623-632. doi:10.1128/JB.00661-15
48. Vetting MW, Yu M, Rendle PM, Blanchard JS. The substrate-induced conformational change of Mycobacterium tuberculosis mycothiol synthase. *J Biol Chem*. 2006;281(5):2795-2802. doi:10.1074/jbc.M510798200
49. Dopkins BJ, Tipton PA, Thoden JB, Holden HM. Structural Studies on a Glucosamine/Glucosaminide N-Acetyltransferase. *Biochemistry*. 2016;55(32):4495-4508. doi:10.1021/acs.biochem.6b00536
50. Reith J, Mayer C. Characterization of a glucosamine/glucosaminide N-acetyltransferase of Clostridium acetobutylicum. *J Bacteriol*. 2011;193(19):5393-5399. doi:10.1128/JB.05519-11

51. Stover CK, de la Cruz VF, Fuerst TR, et al. New use of BCG for recombinant vaccines. *Nature*. 1991;351(6326):456-460. doi:10.1038/351456a0
52. Liu F, Yang M, Wang X, et al. Acetylome Analysis Reveals Diverse Functions of Lysine Acetylation in Mycobacterium tuberculosis. *Mol Cell Proteomics MCP*. 2014;13(12):3352-3366. doi:10.1074/mcp.M114.041962
53. Roussin M, Salcedo SP. NAD+-targeting by bacteria: an emerging weapon in pathogenesis. *FEMS Microbiol Rev*. Published online July 5, 2021:fuab037. doi:10.1093/femsre/fuab037
54. Kim YJ, Lee SH, Jeon SM, et al. Sirtuin 3 is essential for host defense against Mycobacterium abscessus infection through regulation of mitochondrial homeostasis. *Virulence*. 2020;11(1):1225-1239. doi:10.1080/21505594.2020.1809961
55. Robert X, Gouet P. Deciphering key features in protein structures with the new ENDscript server. *Nucleic Acids Res*. 2014;42(Web Server issue):W320-324. doi:10.1093/nar/gku316

SUPPLEMENTARY MATERIALS

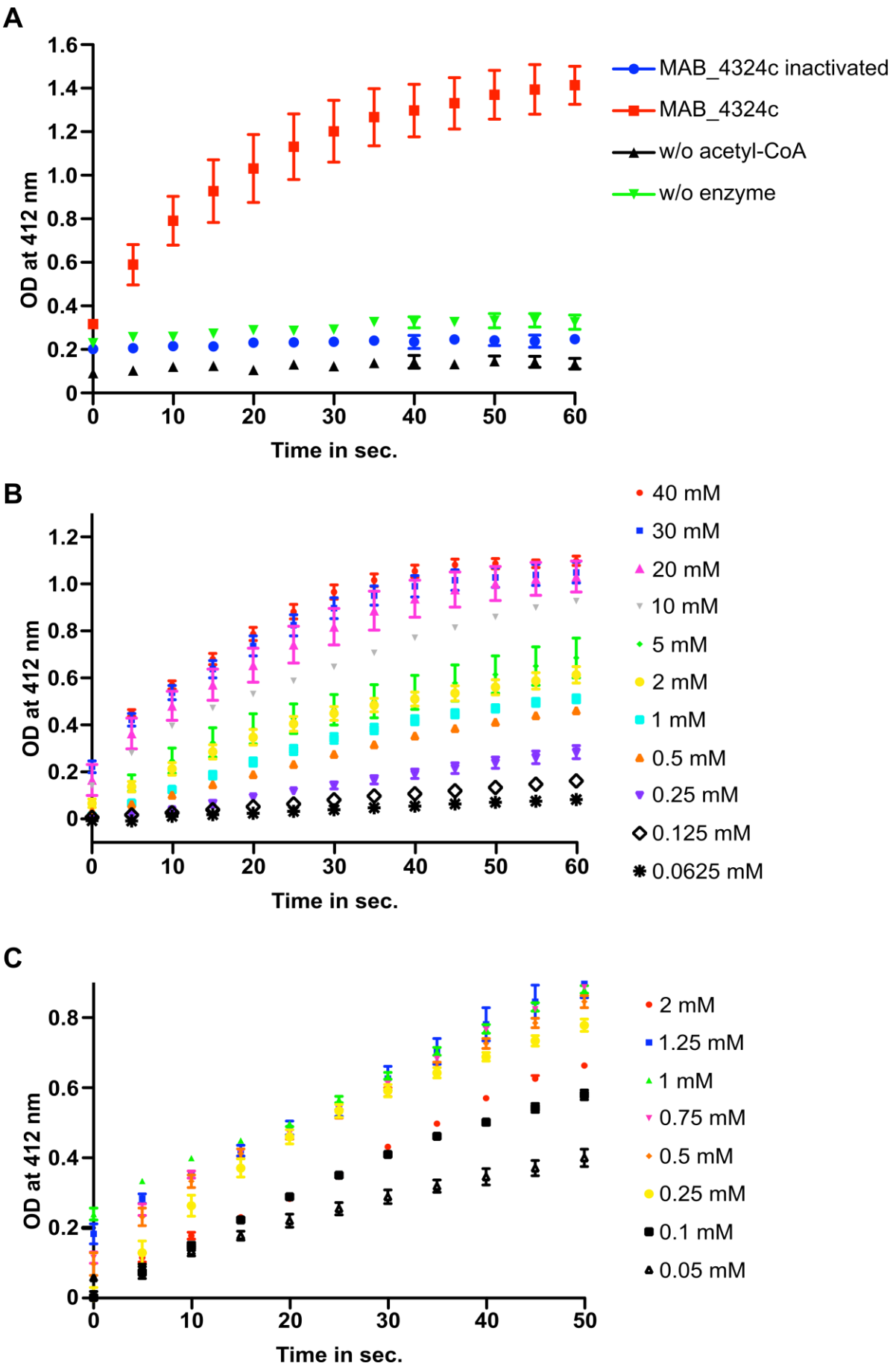

Figure S1: Measurement of the MAB_4324c dependent *N*-acetyltransferase activity.

A-The figure displays the control experiments, which demonstrate that the *N*-acetyltransferase reaction is enzyme dependent. The curves represent the raw data of the monitoring of the optical density at 412 nm over time reflecting the *N*-acetyltransferase activity of MAB_4324c (red dots) at 0.5 µM in presence of 0.1 mM acetyl-CoA, 1 mM spermidine and 0.1 mM DTNB. Control experiments were performed with 0.5 µM inactivated enzyme (blue dots), heated 30 min at 95°C before the reaction as well as a reaction without all the components but acetyl-CoA (black dots) or a reaction with all the components but enzyme (green dots). Experiments performed in triplicate were recorded using a NanoPhotometer® N60 (IMPLEN) and error bars represent the standard error.

B-Raw data of the monitoring of the optical density at 412 nm over time reflecting the *N*-acetyltransferase activity of MAB_4324c (0.25 µM) in presence of varying concentrations of spermidine (0.062 mM to 40 mM) and constant concentration of acetyl-CoA (0.5 mM). For each spermidine concentration a background reaction corresponding to all the components but the enzyme was recorded and these values were subtracted from the recorded values corresponding to the reaction in presence of the enzyme. The data are from triplicate and error bars correspond to the standard error. Initial velocities were calculated with data from the first 35 seconds.

C-Raw data of the monitoring of the optical density at 412 nm over time reflecting the *N*-acetyltransferase activity of MAB_4324c (0.25 µM) in the presence of varying concentrations of acetyl-CoA (0.05 mM to 2 mM) and constant spermidine concentration (40 mM). For each acetyl-CoA concentration a background reaction corresponding to all the components but the enzyme was recorded and these values were subtracted from the recorded values corresponding to the reaction in presence of the enzyme. All experiments were performed in triplicate and error bars correspond to the standard error. Initial velocities were calculated with data from the first 35 seconds.

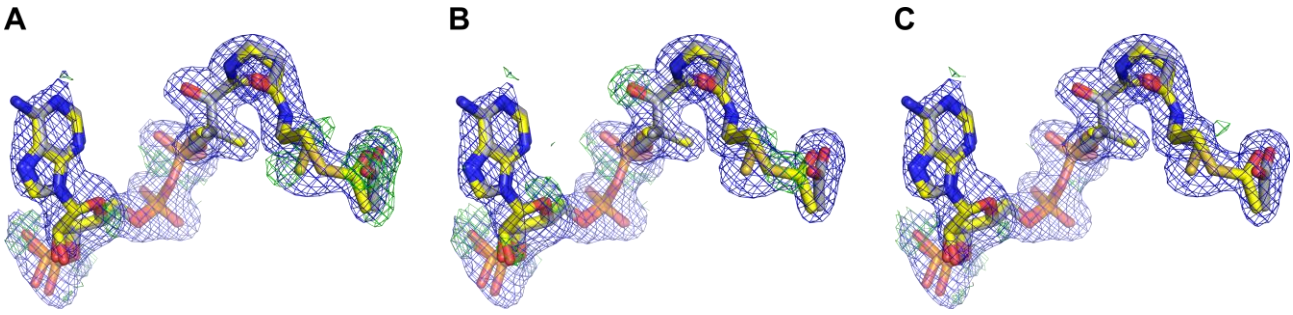

Figure S2: Modelling and refinement of the ligands

The figure depicts the strategy of the acetyl-CoA/CoA/acetate groups refinement. In the three panels acetyl-CoA is in yellow stick, CoA and acetate groups are in grey and the 2Fo-Fc map is in blue and contoured at a level of 1 sigma. The three Fo-Fc maps are in green and contoured at a level of 3 sigma. Panel A shows the map after refinement where acetyl-CoA was set to an occupancy of 1,

while in panel B the occupancy of the acetate group and CoA was set to 1. Panel C shows the acetyl-CoA, acetate and CoA were refined with an estimated occupancy of 0.5. The comparison of three Fo-Fc maps attests that the modeling and refinement strategy of the final model deposited at the PDB and illustrated in panel C was the most adapted.

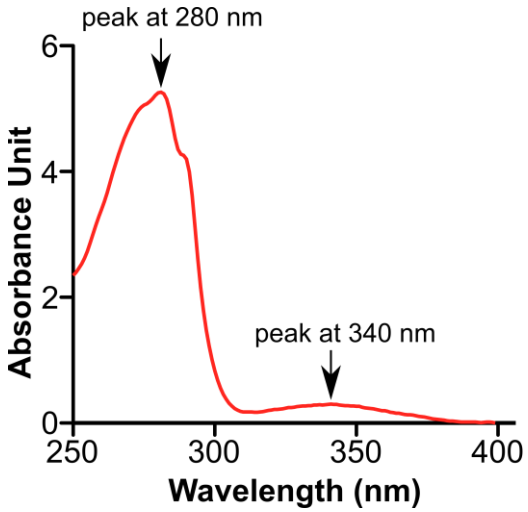

Figure S3: UV spectrum of pure MAB_4324c expressed in *E. coli*

The UV spectrum was acquired on a NanoPhotometer® N60 (IMPLEN). Two major absorption peaks are observed: one with 5.42 absorption units (AU) at 280 nm and a second one with 0.46 AU at 340 nm. Given the MAB_4324c extinction coefficient, 80 440 M^{-1} cm^{-1} and the one of NADH/NADPH, 6220 M^{-1} cm^{-1}, we could estimate the concentration of MAB_4324c to 67 µM and NADH/NADPH to 73 µM. This is strongly indicating that the protein is fully bound to the reduced form of nicotinamide after purification.

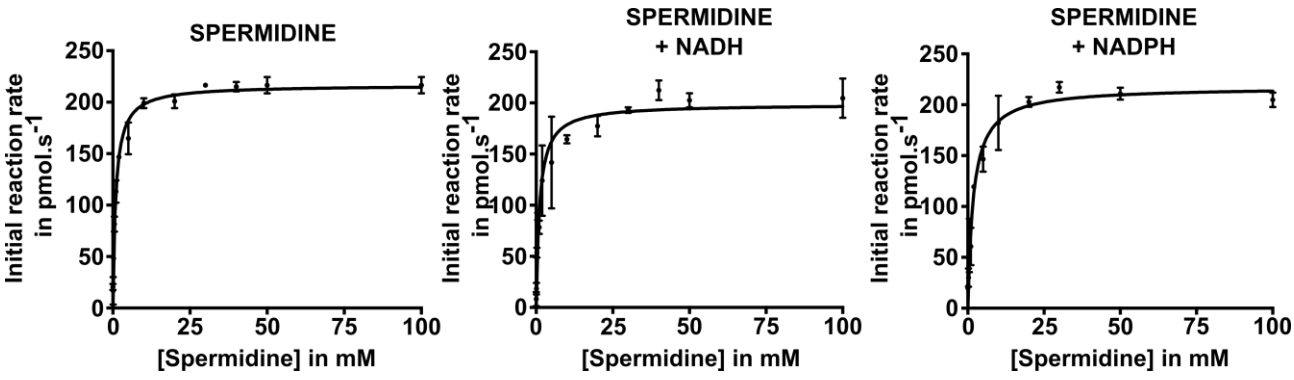

Figure S4: NADH or NADPH do not modulate MAB_4324c enzymatic activity

The figure displays the Michaelis-Menten curves that were used to determine the kinetic constants for spermidine in the presence of 0.5 mM of acetyl-CoA and with 0.25 µM MAB_4324c. The left panel is for MAB_4324c without nicotinamide, middle and right panels are for the reactions

performed in presence of 100 μM of NADH and NADPH respectively. For each spermidine concentration a background reaction corresponding to all the components but the enzyme was recorded and these values were subtracted from the recorded values corresponding to the reaction in presence of the enzyme. The data are from two independent reactions and error bars correspond to the standard error. The kinetic constants are reported in Table S1.

Table S1. Kinetic parameters of MAB_4324c in presence of NADH and NADPH.

Substrates	V_{max} (pmol.s^{-1})	K_M (μM)	k_{cat} (s^{-1})	K_M/k_{cat} (M^{-1} s^{-1})
Spermidine	216.6±3.4	0.95 10^3±0.1	0.86 10^{-3}±0.01 10^{-3}	1.1
Spermidine+NADH	198.7±7.6	1.13 10^3±0.2	0.79 10^{-3}±0.03 10^{-3}	1.4
Spermidine+NADPH	217.5±6.9	1.85 10^3±0.3	0.87 10^{-3}±0.03 10^{-3}	2.12

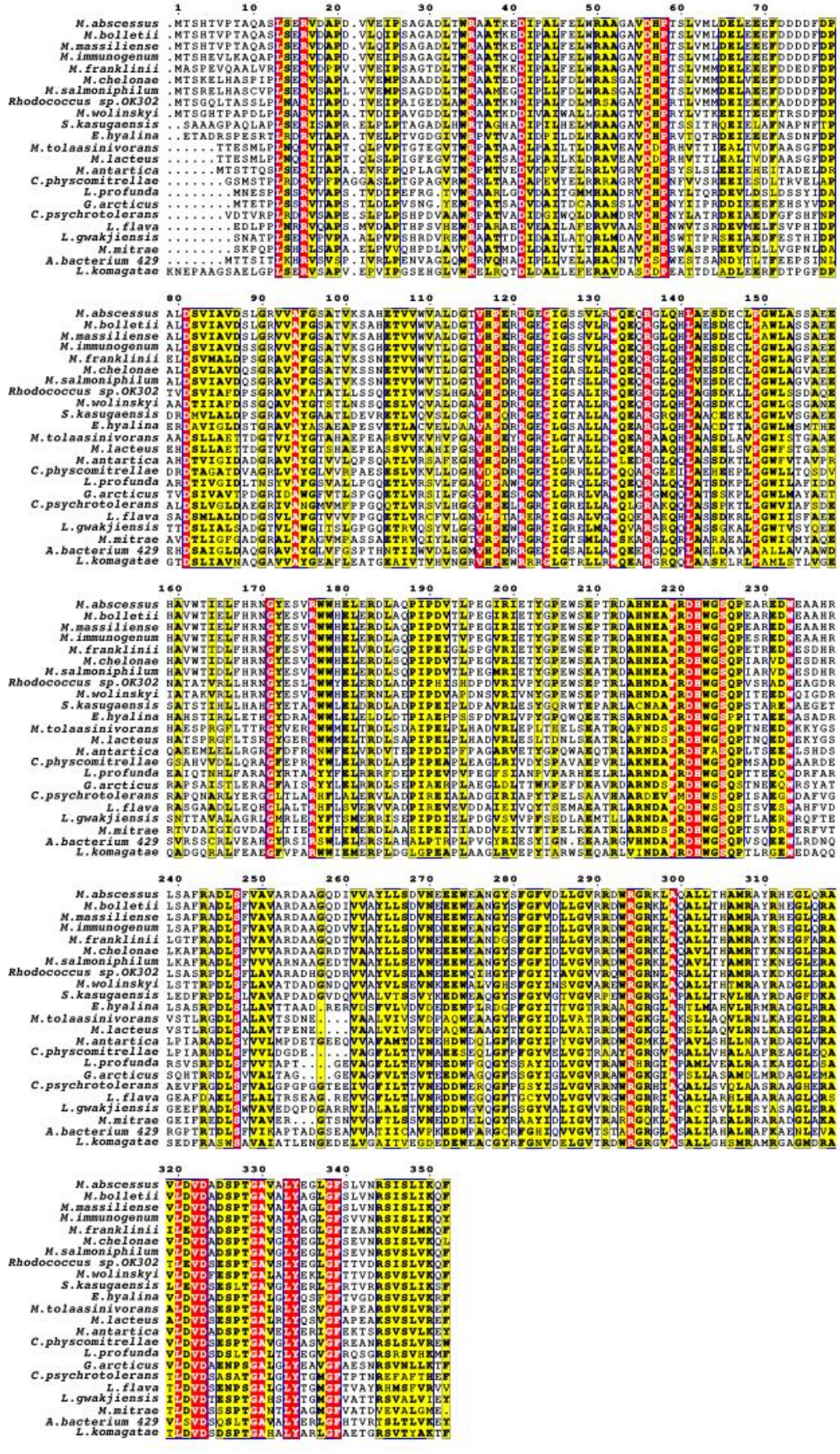
M.abscessus
M.bolletii
M.massiliense
M.immunogenum
M.franklinii
M.chelonae
M.salmoniphilum
Rhodococcus sp.OK302
M.wolinskyi
S.kasugaensis
E.hyalina
M.tolaasinivorans
M.lacteus
M.antartica
C.physcomitrellae
L.profunda
G.arcticus
C.psychrotolerans
L.flava
L.gwakjiensis
M.mitrae
A.bacterium 429
L.komagatae

Figure S5: Multiple sequence alignments of the MAB_4324c orthologues

The sequences of the MAB_4324c orthologues were retrieved with the HMMER server (http://hmmer.org/). Some of the sequences sharing more than 40% protein sequence identity were selected and realigned using the ClustalX software. The alignment was then generated with ESPript (https://espript.ibcp.fr/ESPript/ESPript/). The red and yellow colors indicate strict protein sequence identity conservation or similarity respectively. These protein sequences correspond to the following Uniprot (https://www.uniprot.org/) entries: B1MJN9 for *Mycobacterium abscessus sensu stricto*, A0A1N5X9F8 for *Mycobacterium bolletii*, A0A1U3WRU2 for *Mycobacterium massiliense*, A0A7V8RYX2 for *Mycobacterium immunogenum*, A0A1S1M967 for *Mycobacterium chelonae*, A0A4R8SHM6 for *Mycobacterium salmoniphilum*, A0A4R5PCD3 for *Mycobacterium franklinii*, A0A235FHP5 for *Rhodococcus sp.* OK302, A0A1X2F0T9 for *Mycobacterium wolinskyi*, A0A4Q9HX52 for *Streptomyces kasugaensis*, A0A7L5AGZ4 for *Marisediminicola antarctica*, A0A401YSZ2 for *Embleya hyalina*, A0A3L7A326 for *Mycetocola tolaasinivorans*, A0A1X9LGC8 for *Cnuibacter physcomitrellae*, A0A542Y663 *Leucobacter komagatae*, A0A3L7ARX6 for *Mycetocola lacteus*, A0A5C8URY9 *Lacisediminihabitans profunda*, A0A4Q9GUC3 for *Glaciihabitans arcticus*, A0A1G9AKS2 for *Cryobacterium psychrotolerans*, A0A4S1E912 for *Alcaligenaceae bacterium* 429, A0A2P8GRY7 for *Labedella gwakjiensis*, A0A4Y9R9U9 for *Leifsonia flava* and A0A5C8HQH6 for *Microbacterium mitrae*.

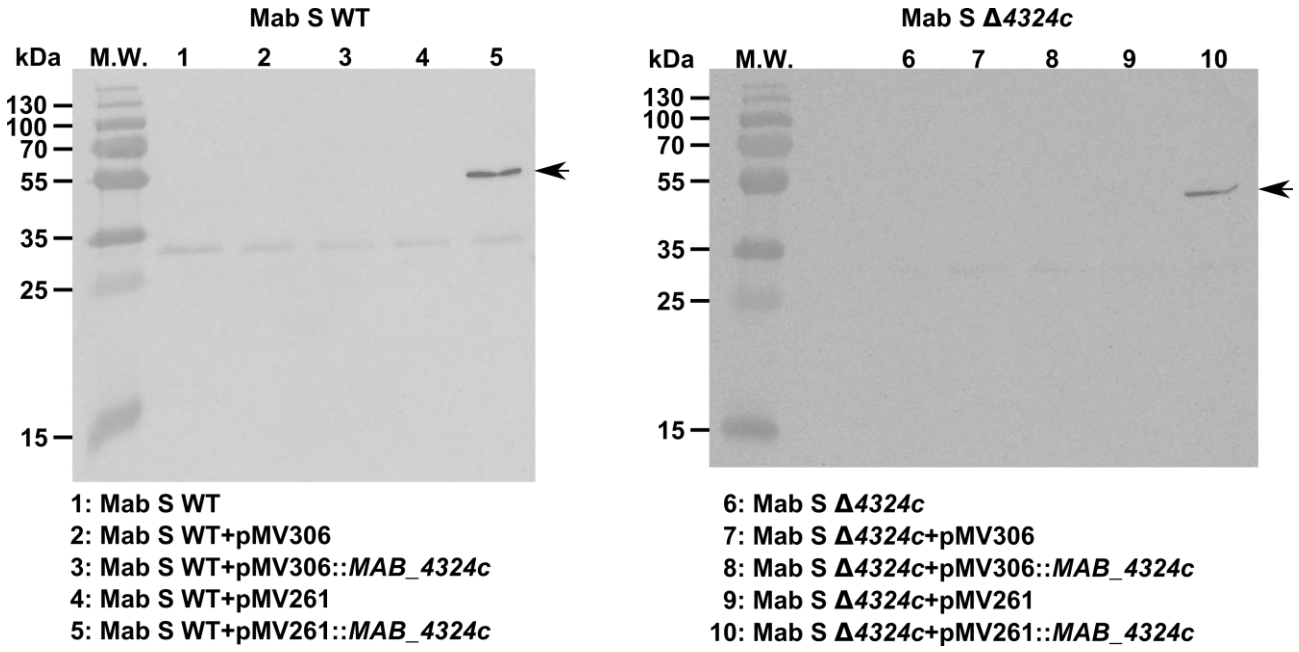

Figure S6: Western blot confirming the expression of MAB_4324c

Protein expression assessment of MAB_4324c in the parental (Mab S WT) and knockout strains (Mab S Δ*4324c*). The Western blotting revealed with anti-Strep tag primary antibodies attests to the expression of MAB_4324c in both strains transformed with pMV261::*MAB_4324c* (wells 5 and 10). Expression trials with the integrative pMV306::*MAB_4324c* were not successful (wells 4 and 8). Strains transformed with the empty plasmids were included as negative controls.

Table S2. Determination of the MIC_{99}

Antibiotics	MIC ($\mu g.mL^{-1}$) Mab S wild-type	MIC($\mu g.mL^{1}$) Mab S Δ*MAB_4324c*
Bedaquiline	0.16	0.16
Kanamycin B	25	25
Amikacin	50	50
Tigecycline	5	5
Clofazimine	3.1	1.5
Imipenem	32-64	32-64
Ethambutol	>100	>100
Cefoxitin	61.2	61.2
Ciprofloxacin	61.2	61.2
Vancomycin	>250	>250

MIC of the different antibiotics were determined as described in the Materials and Methods.

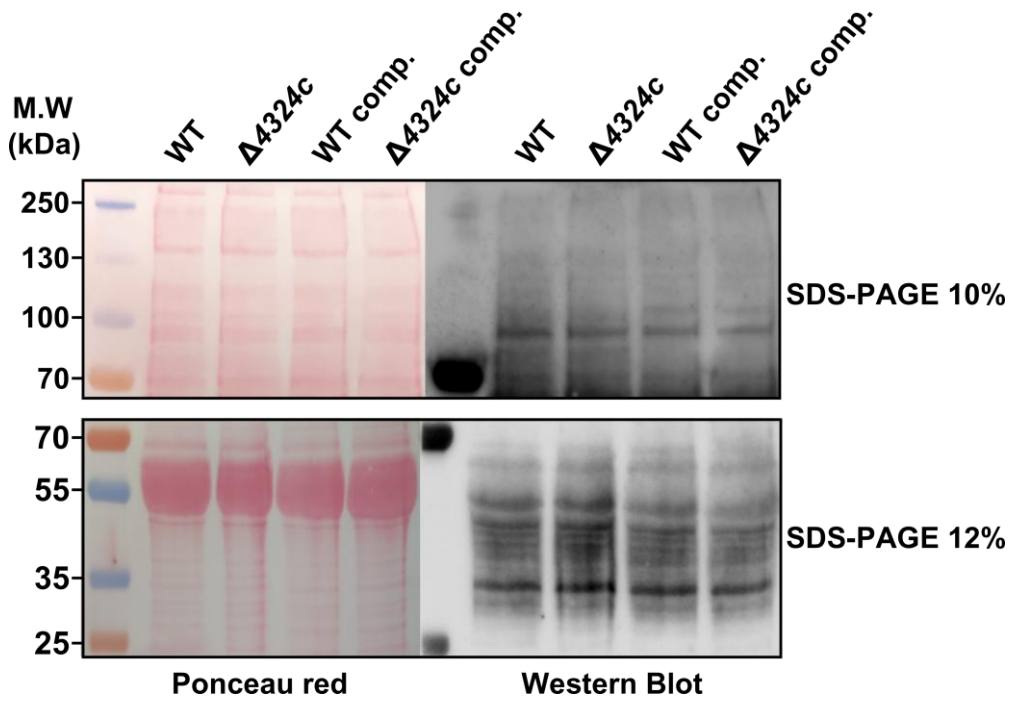

Figure S7: *M. abscessus* acetylome revealed by an anti-acetyl lysine antibody

Comparison of the protein lysine acetylation pattern of the WT, WT overexpressing MAB_4324c WT comp.), Δ*4324c* and Δ*4324c* complemented strains (Δ*4324c* comp.). The lysine acetylome was detected with a pan anti-acetyl lysine primary antibody (abcam 21623) and revealed with an anti-rabbit secondary antibody produced in goats and coupled to the horseradish peroxidase. On the left is shown the membrane after transfer and colored by ponceau red while on the right is the immunoblot revealed by chemiluminescence. 100 µg of total protein were loaded on the 10% SDS-PAGE for high molecular weight (HMW) proteins and 12% SDS-PAGE for proteins of medium molecular weight (MMW) proteins. The primary antibody was diluted 500 and 1000 times for HMW and MMW proteins respectively while the secondary antibody was diluted 5000 and 10000 times. Only a very weak signal could be detected for proteins with a molecular weight below 25 kDa (not shown).